Smell-induced gamma oscillations in human olfactory cortex are required for accurate perception of odor identity

Qiaohan Yang*[1], Guangyu Zhou*[1], Torben Noto[1], Jessica Templer[1], Stephan Schuele[1], Joshua Rosenow[2], Gregory Lane[1], Christina Zelano[1]

[1:] Department of Neurology, Feinberg School of Medicine. Northwestern University. 320 E Superior Ave, Chicago IL. 60611

[2:] Department of Neurosurgery, Feinberg School of Medicine. Northwestern University. 320 E Superior Ave., Chicago IL. 60611

***, corresponding author: guangyu.zhou@northwestern.edu**

This work was funded by National Institutes of Health (NIDCD) grants R01-DC-016364 and R01-DC-018539 to C.Z.

The authors declare that they have no competing interest.

Abstract

Studies of neuronal oscillations have contributed substantial insight into the mechanisms of visual, auditory and somatosensory perception. However, progress in such research in the human olfactory system has lagged behind. As a result, the electrophysiological properties of the human olfactory system are poorly understood, and in particular, whether stimulus-driven high frequency oscillations play a role in odor processing is unknown. Here, we used direct intracranial recordings from human piriform cortex during an odor identification task to show that three key oscillatory rhythms are an integral part of the human olfactory cortical response to smell: odor induces theta, beta and gamma rhythms in human piriform cortex. We further show that these rhythms have distinct relationships with perceptual behavior. Odor-elicited gamma oscillations occur only during trials in which the odor is accurately perceived, and features of gamma oscillations predict odor identification accuracy, suggesting they are critical for odor identity perception in humans. We also found that the amplitude of high-frequency oscillations is organized by the phase of low frequency signals shortly following sniff onset, only when odor is present. Our findings reinforce previous work on theta oscillations, suggest that gamma oscillations in human piriform cortex are important for perception of odor identity, and constitute a robust identification of the characteristic electrophysiological response to smell in the human brain. Future work will determine whether the distinct oscillations we identified reflect distinct perceptual features of odor stimuli.

Introduction

Oscillations are ubiquitous across mammalian brain networks [1,2,11,3–10] and studies on their spectrotemporal dynamics have contributed important insight into the mechanisms underlying visual, auditory, and somatosensory perception [10,12–16]. Some of the earliest recordings of brain oscillations occurred in the olfactory system of hedgehogs [17], leading to decades of highly productive animal research on oscillations in the mammalian olfactory system with significant work in rabbit and cat piriform [18–22] and more recently mainly focusing on the rodent olfactory bulb [5,8,31–40,23,41–43,24–30]. However, 80 years later, we still lack understanding of the spectral and temporal dynamics of these oscillations in olfactory processing in the human brain, particularly in higher frequency ranges including beta and gamma.

Gamma oscillations, which comprise the synchronized rhythmic patterns of spiking and synaptic inhibition, have been established as an important mechanism in sensory cortical processing in the mammalian brain [44,45]. In the visual cortex, gamma oscillations are locally generated and reflect low-level stimulus attributes [46] including grating size, contrast, spatial structure and color [47–50], and are thought to support visual perception by synchronizing the processing and transfer of information within and across areas of visual cortex [51–53]. Similarly, in the auditory cortex, locally generated gamma oscillations may provide a mechanism to integrate neurons according to the similarity of their receptive fields [54], and are involved in pitch perception and sound discrimination [55,56].

In the olfactory system, odor-driven increases in beta and gamma oscillations have not been consistently identified in direct recordings from human piriform (olfactory) cortex, which has been found to exhibit low frequency oscillations in response to odor [57]. However, in mammals and insects, the cellular and network processes underlying gamma oscillations in the olfactory bulb and cortex have been studied extensively [19,29,40,58–63], and more recent work has begun to provide insight on their functional role as well [23,26,32,33,36,37,40,64], suggesting involvement in organization of sensory information to enable fine odor discrimination and identification [23,65–69]. In addition to gamma oscillations, beta and theta oscillations have been extensively studied in the mammalian olfactory system, and are involved in olfactory learning and respiratory tracking, respectively [18,27,70,71,28,30,33,36,38,40,64,65]. Thus theta, beta and gamma oscillations constitute three key rhythms that have functional significance for olfactory processing in mammals [8]. However, against this background of extensive animal work, the electrophysiological underpinnings of the human olfactory system are vastly understudied. Only a few intracranial studies have directly measured odor-induced oscillations in the human brain; in the amygdala [72–76] and piriform cortex [57]. Human piriform recordings suggest an important role for low frequency (< 8 Hz) oscillations in olfactory processing [57]; theta oscillations were consistently found in piriform cortex within 200 ms of sniff onset during an odor detection task, and their features could be used to decode odor identity. However, the full spectral characteristics of early and later emerging odor responses in human olfactory cortex remain unknown. Furthermore, the functional role of high frequency oscillations in human piriform cortex is virtually unexplored.

In this study, we used stereotactic intracranial electroencephalography (iEEG) to test three main hypotheses about neural responses in human piriform cortex during an olfactory identification task. First, based on the fundamental role of gamma oscillations in human sensory perception and the established rhythms in the rodent olfactory system, we hypothesized that odors would induce theta beta and gamma oscillations in human piriform cortex. Second, based on the fact that olfactory oscillations are modulated by sniffing [26,58,62,63,77–79], which is inextricably linked to odor onset times, we hypothesized that the timing of responses relative to sniff onset would vary across the different frequency bands. Third, based on established links between gamma/beta oscillations and sensory coding [27,30,32,33,35,36,38,64], and the fact that activity in rodent piriform cortex can be used to decode odor identity [80–82], we hypothesized that human piriform beta and gamma oscillations would emerge only during trials where odors were accurately identified, and that features of their oscillatory rhythms would predict odor identification accuracy.

Our results show that odors elicit a stereotyped oscillatory response in human piriform cortex that is consistent in timing and frequency composition across subjects: Immediately following odor onset, early theta increases are quickly followed by gamma and beta increases. The phase of early low frequency responses drives the amplitude of high frequency rhythms only when odor is present. Finally, the distinct oscillatory rhythms we identified were differentially related to behavioral performance, suggesting that these rhythms could potentially give rise to non-interfering representations of different features of odor stimuli [81,82], though future work is needed to test this hypothesis.

Results

To examine odor-driven oscillations in human olfactory cortex, we recorded local field potentials from 7 participants who took part in an odor identification task. Each participant's clinical electrode coverage included piriform cortex (**Fig 1A**). The olfactory task was performed during clinical recording of ongoing electrophysiological activity, at sampling rates ranging between 500 to 2000 Hz, using a 256-channel clinical EEG acquisition system (Nihon Kohden). Each trial began with an auditory cue signaling that odor would be presented, and providing the potential identity of the odor (rose or mint). After a jittered delay (3–7 s), odor was presented to the participant while sniff onset was precisely measured via a pressure sensor at the nose (Salter Labs). On each trial, participants identified the odor by indicating whether or not it matched the identity prompt (**Fig 1B**). To isolate effects driven by odor from those driven by inhalation, which also impacts oscillations in human piriform cortex [78,83–85], we analyzed and directly compared LFPs during inhalations that contained odor and those that did not, resulting in two experimental conditions: odor and no-odor (**Fig 1B**, areas shaded in pink and blue).

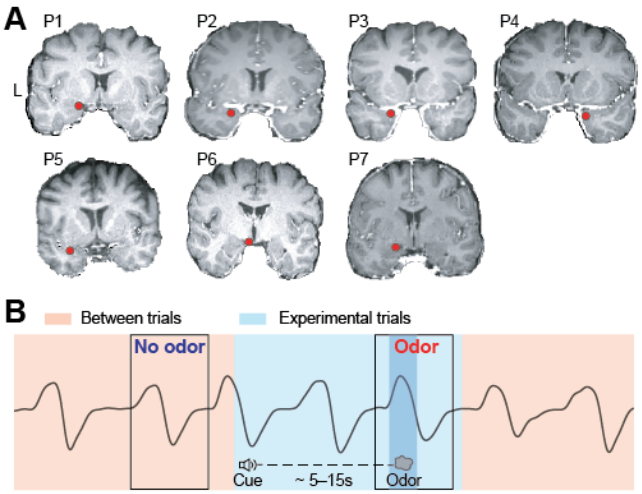

Fig 1. Electrode contact locations and experimental design. (A) The location of the piriform cortex electrode contact (red dot) is shown on each participant's (P1–P7) brain image. L, left hemisphere. (B) Schematic illustration of the olfactory task, showing odor and no-odor conditions drawn on an illustrative breathing signal (black line). The light blue area indicates experimental trials (starting from cue delivery to the end of the breathing cycle in which odor was delivered), and the pink area indicates between trials. The black boxes indicate the analysis time windows for odor and no-odor trials. The darker blue area indicates odor delivery.

Odor elicits oscillations in theta, beta and gamma frequency bands in human piriform cortex

To test the hypothesis that odor elicits LFP oscillations in the theta, beta and gamma frequency bands in human piriform cortex, we first conducted a time-frequency analysis combining data from all trials and participants. We computed spectrograms aligned to sniff onset, for odor and no-odor conditions separately. In the odor condition, we found statistically significant increases in theta, beta and gamma frequency bands (**Fig 2A**, left

panel) (theta peak: 4.72 Hz, max z score = 14.07; beta peak: 18.98 Hz, max z score = 8.11; gamma peak: 84.94 Hz, max z score = 4.88). In the no-odor condition, we found smaller but significant increases in theta only (**Fig 2A**, middle panel; peak: 4.02 Hz, max z score = 3.44). To quantify the difference between odor and no-odor conditions, we conducted a direct statistical comparison by permuting condition labels to generate a map of z-normalized amplitude differences (**Fig 2A**, right panel). We found that theta, beta and gamma amplitudes were significantly higher in the odor compared to the no-odor condition (permutation test; $P < 0.05$, FDR corrected).

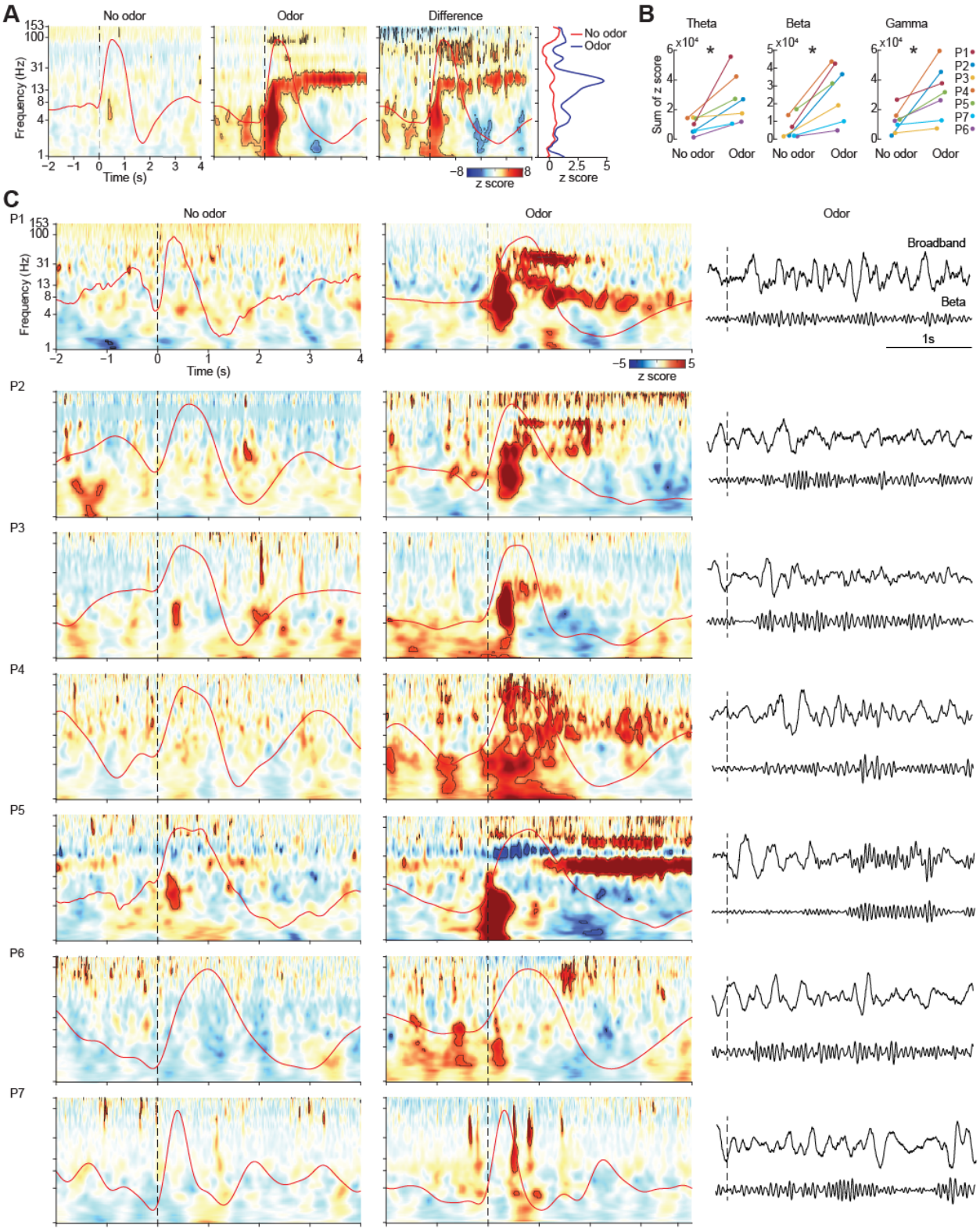
A
No odor
Odor
Difference
Frequency (Hz)
Time (s)
z score
No odor
Odor
B
Theta
Beta
Gamma
Sum of z score
No odor
Odor
P1
P2
P3
P4
P5
P6
C
P1
P2
P3
P4
P5
P6
P7
Broadband
Beta
1s

153

Fig 2. Odor induces theta, beta and gamma oscillations in human piriform cortex. (A) Results from combined analysis showing z-normalized amplitude spectrograms for no-odor and odor conditions (left and middle panels), and the difference between the two conditions (right panel). Average respiratory signal is shown on each panel (overlaid red line). Dashed line represents inhale onset. For odor and no-odor spectrograms, the black contour lines indicate statistical significance of permutation tests against pre-cue baseline ($P < 0.05$, FDR corrected). For the difference spectrogram, the black contour lines indicate statistical significance of permutation of condition labels ($P < 0.05$, FDR corrected). The far-right panel shows average z scores from 0–4 s post sniff across frequencies for odor and no-odor trials. B) Individual theta, beta and gamma summed magnitudes over 0–2 s post sniff. Each dot represents data from a single participant, and lines connect data within the same participant. Asterisk indicates statistical significance (two-tailed paired t test; $P < 0.05$). (C) Z-normalized amplitude spectrograms for each participant for no-odor (left) and odor (middle) conditions, with the average respiratory signal shown on each panel (overlaid red line). Dashed lines represent inhale onset. Black contour lines indicate statistical significance of permutation tests against pre-cue baseline ($P < 0.05$, FDR corrected). Raw broadband and beta (13–30 Hz) time series of a representative trial is shown on the right. The source data for panels (A)–(C) are available in S1 Data.

To confirm our findings at the individual level, we next computed sniff-aligned spectrograms, in each participant separately (**Fig 2B–C**). To quantify responses in each participant, we used standard human EEG frequency band definitions (theta: 4–8 Hz; beta: 13–30 Hz; gamma: > 30 Hz), and looked for responses occurring within these standard frequency ranges in each participant. We computed a direct statistical comparison between the two conditions across participants, which showed that amplitudes in these three frequency bands were significantly stronger across participants during the odor compared to the no-odor condition (**Fig 2B**) (two-tailed

179 paired t test, theta: T_6 = 3.19, P = 0.0187; beta: T_6 = 4.17, P = 0.0059; gamma: T_6 =
180 2.98, P = 0.0245). Notably, in every single participant, theta, beta and gamma
181 amplitudes were larger during the odor compared to the no-odor condition (**Fig 2B**,
182 each dot is the result from one participant and lines connect same-participant results
183 between conditions). Though there was some variation across individuals in the
184 frequency of responses, these effects were evident in the individual spectrograms of
185 most participants (**Fig 2C;** black outlines indicate statistical significance via permutation
186 test; $P < 0.05$, FDR corrected), and in the minimally-processed signals shown next to
187 each individual spectrogram (**Fig 2C**, right). In each participant, theta, beta and gamma
188 responses were maximal inside piriform cortex, with significantly reduced responses
189 outside of piriform on the same depth wire (two-tailed paired t test; theta: P = 0.0045, T_6
190 = 4.42; beta: P = 0.014, T_6 = 3.44; gamma: P = 0.0070, T_6 = 4.02) (**S1 Text**; **S1 Fig 3A**).
191 To further visualize the spatial distribution of responses in each frequency band, we
192 created heat maps of responses across all implanted electrodes in all participants,
193 projected onto an axial slice through piriform cortex (**S1 Fig 3B**). This allowed
194 visualization of response magnitudes in the anterior-posterior direction, with the
195 superior-inferior axis flattened. A hot spot of increased activity can be seen
196 corresponding to piriform cortex (**S1 Fig 3B**, pink boxed areas; axial slice contains
197 piriform cortex).

198 To address the possibility that the responses we observed were due to the steep slopes
199 of sensory-evoked potentials, we conducted an analysis to separate the spectrograms
200 into odor-evoked and odor-induced effects [86–88]. In this analysis, the odor-evoked
201 spectrogram includes only the phase-locked power, which contributes to the sensory-

evoked potential, whereas the odor-induced spectrogram includes only the non-phase-locked power, which is oscillatory and is not related to the ERP [89,90] (see methods). Results of this analysis showed that odor-induced oscillations were not eliminated when the phase-locked components of the signal were removed (**S1 Fig 1**) and thus were not due to the steep slope of sensory-evoked potentials.

In rodents, odor has been shown to elicit responses in multiple gamma subbands [8,64,91]. To examine gamma effects more closely and to look for multiple gamma sub-bands in humans, we re-computed individual spectrograms using a linear, as opposed to log, frequency scale. We found that most subjects showed odor-induced oscillations right around or just below 30 Hz. Most subjects also showed a higher frequency broadband response, around 90–150 Hz (**S1 Fig 2**).

Together, these results suggest that odor consistently induces distinct theta, beta and gamma oscillations in human piriform cortex.

The time course of olfactory cortical oscillations varies across frequency bands

The spectrograms in **Fig 2** showed apparent variable time courses of oscillations relative to sniff onset across frequency bands (**Figs 2A and 2B**). Theta appeared to emerge and dissipate soonest, with beta and gamma emerging later and persisting longer. To quantify these differences, we conducted a series of analyses to characterize the timing of responses across frequency bands. These included a percent-change analysis to examine oscillatory increases over time, a bootstrapping analysis to

minimize potential impact of noisy trials, a cluster-based analysis to quantify the exact timing and magnitude of continuously significant increases in oscillatory amplitude, and a circular-distribution analysis to examine oscillatory peaks over respiratory phase.

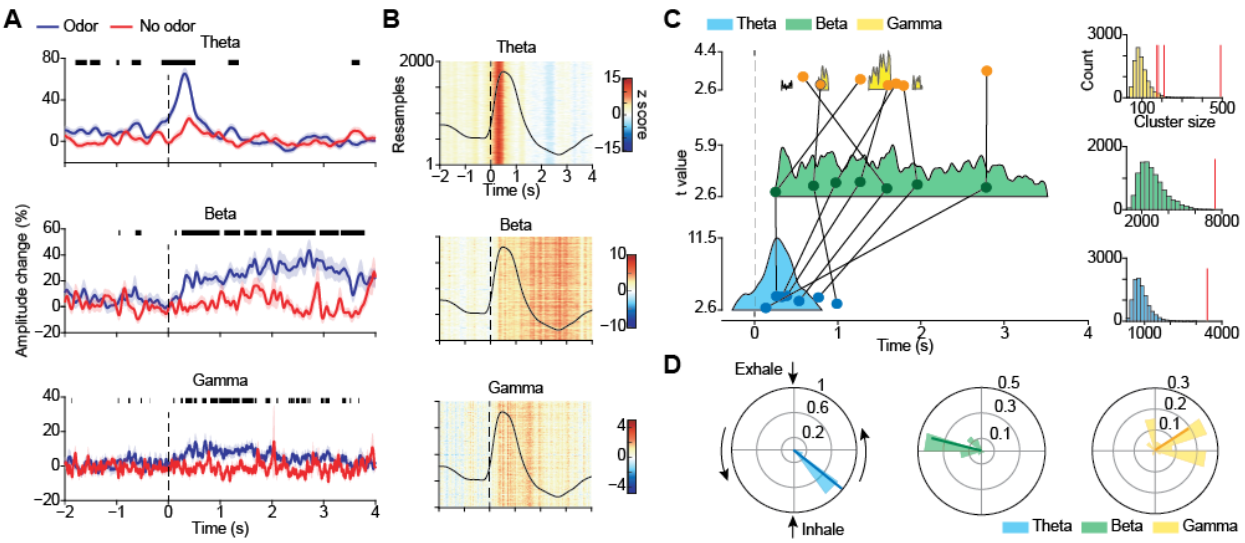

Fig 3. Odor-induced theta, beta and gamma oscillations have different time courses relative to sniff onset. (A) Percent-amplitude-change time series for odor (blue line) and no-odor (red line) conditions for each frequency band. Shaded areas indicate one standard deviation from the mean across all trials. Thick black lines above indicate statistically significant differences between conditions (FDR corrected $P < 0.05$, paired t test). (B) Bootstrap colormap of z-normalized amplitude for each frequency band, with results from each repetition stacked along the Y axis. Vertical stripes of consistent color indicate consistent amplitudes across subsampled sets of trials. (C) Colored shaded areas represent clusters of statistical significance of the trial-by-trial baseline-corrected amplitude time series, for each frequency band (cluster correction test $P < 0.05$, corrected). Upper boundaries of the shaded areas represent the t statistic from the one-sample t test of baseline-corrected amplitude at each time point against 0. Scales for t statistics are shown to the left of each cluster. Overlaid darker dots indicate the average timing of the bootstrapped distribution of peak amplitude occurrence for each frequency band, for each participant. Each dot represents data from one participant. Dots from the same participant are connected by black lines. On the

right, cluster masses in relation to the permuted null distribution for each frequency band are shown, with actual values represented by the vertical red line. (D) Respiratory phase angle distributions corresponding to bootstrapped peak amplitudes for each frequency band. Scale of the polar histogram represents pdf of the distribution. Darker lines overlaid on the distribution indicate the mean vector of the phase distribution. Angle and radius represent averaged phase angle and PLV value respectively. The source data for panels (A)–(D) are available S2 Data.

In our first analysis, we calculated the percent change in amplitude for each frequency band at each time point, for each condition (**Fig 3A**). This allowed us to determine the timing of the emergence of significant differences between odor and no-odor conditions (two-tailed paired t test; $P < 0.05$, FDR corrected). This analysis showed distinct temporal dynamics of odor responses for each frequency (**Fig 3A**, black lines above each panel). Theta oscillations were the earliest to emerge and dissipate, beginning 126 ms prior to sniff onset and ending 516 ms after sniff onset. Gamma oscillations emerged next, 116 ms after sniff onset, intermittently persisted through exhalation, and dissipated 3678 ms after sniff onset. Beta oscillations emerged last, 144 ms after sniff onset, and persisted longest, ending 3786 ms after sniff onset.

In a second analysis, designed to minimize the contribution of noisy trials and to statistically evaluate the time courses, we tested whether differences in temporal dynamics of responses across frequency bands were stable across resampled sets of trials. We conducted a bootstrapping analysis to create separate profiles of the timing of emergence of responses for each frequency band. We created a z-normalized time series of resampled mean values for each frequency band, represented as a colormap

264 (**Fig 3B**, y-axis is each bootstrap repetition). We found stable time courses across
265 repetitions, indicated by stripes of increased amplitude at particular times for each
266 frequency band. To quantify the timing of amplitude increases, we performed a cluster-
267 based statistical analysis; for each frequency band, we generated a t-statistic at each
268 time point for all z-normalized odor trials, and then conducted a permutation-based
269 analysis to correct for cluster size. We found clusters that corresponded well with the
270 spectrograms shown in Fig 2, with the percent-change analysis, and with the bootstrap
271 analysis (**Fig 3C**). We found one significant cluster for the theta band extending 266 ms
272 pre sniff to 810 ms post sniff (permutation test; $P < 0.0001$), one for the beta band
273 extending from 238 ms to 3524 ms post sniff ($P < 0.0001$), and four separate clusters
274 for the gamma band (326 ms to 452 ms post sniff, $P = 0.0346$; 764 ms to 892 ms post
275 sniff, $P = 0.0145$; 1374 ms to 1642 ms post sniff, $P < 0.0001$; 1902 ms to 2016 ms post
276 sniff, $P = 0.0451$). We subsequently conducted the same bootstrapping analysis at the
277 single subject level, and plotted the average time point of each subject's bootstrapped
278 peak distribution on top of the significant clusters in Fig 3C (see overlayed dots, each
279 representing the peak value for a single participant, with lines connecting each
280 participant's values across frequencies). Although single participant data was more
281 variable, beta and gamma peaks occurred later than theta peaks for almost all subjects.
282 These results suggest that the unique time courses of odor responses across
283 frequencies were unlikely to be caused by noise, spikes, and other artifacts.

284 In a third analysis, designed to account for individual respiratory differences in the time
285 domain, we examined the circular distributions of oscillatory peaks over the respiratory
286 phase. On each repetition of a bootstrapping analysis, the peak amplitude and

corresponding phase angle were calculated from the average LFP and respiratory time series. We found that theta peaks narrowly aggregated at early stages of inhale (mean phase angle = –0.67 rad, PLV = 0.99, Rayleigh's z = 998.05, $P < 0.0001$) (**Fig 3D**, left), consistent with previous findings in humans [57]. By contrast, beta peaks consistently aggregated at the exhale trough (mean phase angle = 2.98 rad, PLV = 0.80, Rayleigh's z = 647.78, $P < 0.0001$) (**Fig 3D**, middle). Gamma peaks were more broadly distributed, with most centered around inhale peak or the transition between inhale and exhale (mean phase angle = 0.57 rad, PLV = 0.63, Rayleigh's z = 401.69, $P < 0.0001$) (**Fig 3D**, right). Combined, these findings suggest that following presentation of odor, theta oscillations increase earlier than beta and gamma oscillations, and that while theta and gamma oscillations are maximal during inhalation, beta oscillations peak during exhale.

Gamma and beta oscillations are required for accurate odor identification.

Piriform cortex has been postulated to be a major driver of gamma oscillations in the brains of rodents [18,92] and cats [19–22,93]. Furthermore, numerous rodent studies suggest that beta and gamma oscillations relate to odor learning and discrimination, through both local odor coding [23,33,35,40,64,94] and recruitment of larger-scale networks [27,30,35–37,64]. We therefore hypothesized that beta and gamma oscillations in human piriform cortex would correlate more strongly with task performance than theta. We conducted three separate analyses to explore the relationship between odor-driven LFP oscillations and odor identification accuracy. These included a time-frequency analysis to look for gross differences between correct and incorrect trials, a correlation analysis to look for a relationship between accuracy and oscillations across trials, and a machine learning analysis to determine whether amplitudes of different frequency responses could predict accuracy.

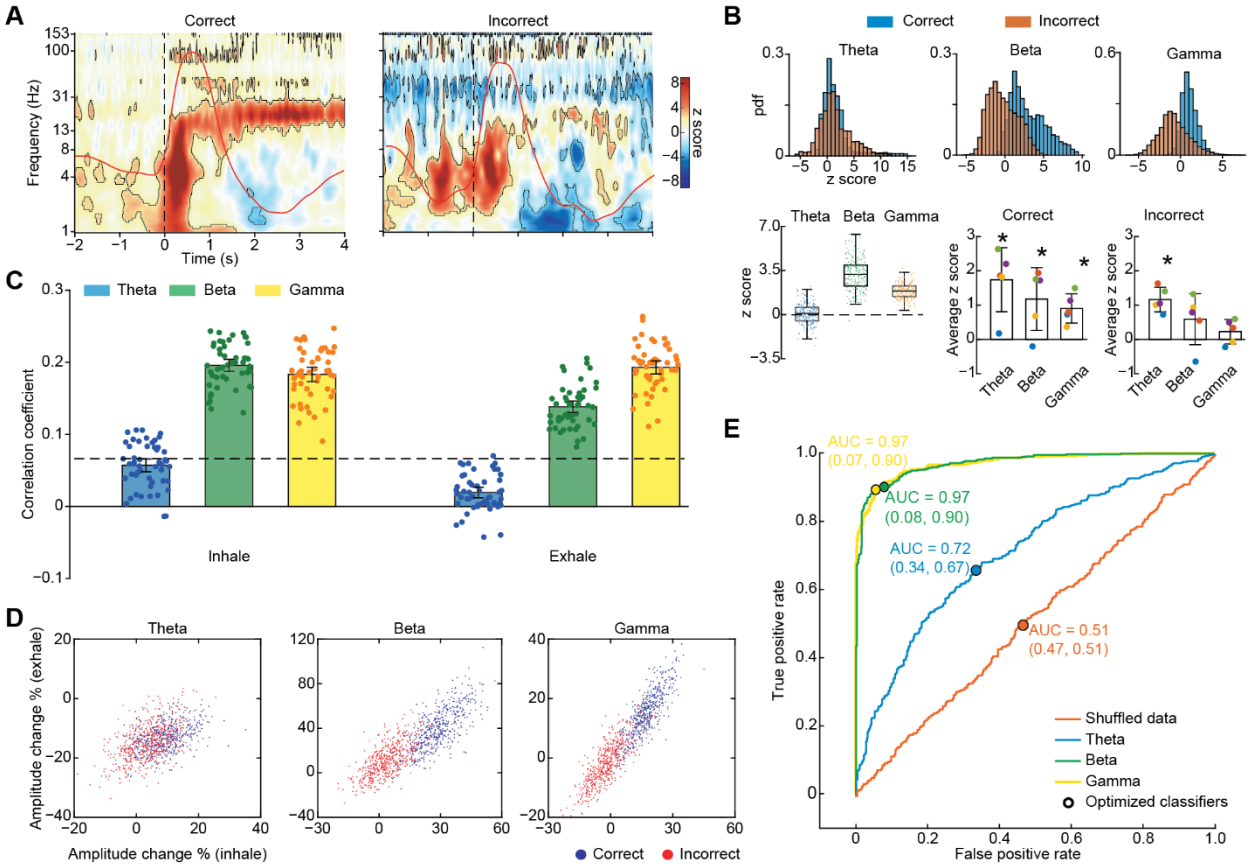

Fig 4. Beta and gamma oscillations predict odor identification accuracy. (A) Z-normalized spectrograms for correct (left) and incorrect (right) trials separately. Averaged respiratory signals are overlayed on each spectrogram (red lines). Dashed lines represent sniff onset. Black contours indicate statistical significance of permutation test against pre-cue baseline ($P < 0.05$, FDR corrected). (B) Amplitudes within each frequency band, for correct and incorrect trials separately. The upper panels show the distribution of z score amplitude values for each trial for the theta, beta and gamma bands, for correct (blue) and incorrect (red) trials. The lower left panel shows box plots for the bootstrapped distributions of the difference between correct and incorrect trials. Boxes represent the 25th to 75th percentile of each distribution, the central marker indicates median, and whiskers extend to the extremes of the data excluding outliers. Colored dots represent raw difference values for each distribution. The lower right panels show individual participant's mean response amplitudes in the theta, beta and gamma bands, for correct and incorrect trials separately. Each dot represents data from a single participant, bars indicate the mean across participants and error bars are standard error across participants. Stars indicate statistical significance

(paired, two-tailed t tests). See Fig 2B for the color code of single participant dots. (C) Bar plots of bootstrapped Pearson's correlation coefficients computed between oscillatory amplitudes and task accuracy for each frequency band, over the inhale and exhale time periods separately. Error bars indicate 95% confidence interval of the mean. Dashed line indicates FDR threshold for significant r value. Dots represent single correlation coefficient calculated from each bootstrap. (D) Scatter plots show bootstrapped percent change relative to baseline for correct and incorrect trials, during inhale and exhale time periods for each frequency band. Each dot is the average result from one bootstrap repetition. (E) Receiver operating characteristic (ROC) curves of linear binary SVM classifier applied to each of the scatter plots in panel C. Black dots represent optimized classifier, area under the curve (AUC) is indicated for each ROC curve. The source data for panels (A)–(E) are available in S3 Data.

First, in a combined time-frequency analysis, we computed odor-onset aligned spectrograms during correct and incorrect trials separately, in order to look for differences across frequency bands. We found that during trials in which the participant correctly identified the odor, there were statistically significant increases in theta, beta and gamma band amplitudes (**Fig 4A**, left panel; $P < 0.05$, FDR corrected). By contrast, during trials in which the participant failed to identify the odor, statistically significant increases were found only in the theta band, with no such increases in the beta or gamma bands (**Fig 4A**, right panel; $P < 0.05$, FDR corrected; **Fig 4B**, upper panels and lower left panel show the distribution of single trial theta, beta and gamma values for correct and incorrect trials). Since most participants performed above chance on the task, there were a larger number of correct trials than incorrect trials (252 versus 71). To account for this difference, we conducted a resampling analysis with 200 repetitions in which correct and incorrect trials were resampled with replacement to include the same

number of trials on each repetition, and we computed the distribution of the differences in amplitude (correct – incorrect) within each frequency band (**Fig 4B**, lower left panel). We found statistically significantly larger responses during correct compared to incorrect trials for beta and gamma bands only, with no significant differences in the theta band. (One-sample t test against 0 for the difference between correct and incorrect trials: theta: $T_{199} = 1.21$, $P = 0.2247$; beta: $T_{199} = 35.55$, $P < 0.0001$; gamma: $T_{199} = 42.61$, $P < 0.0001$. Paired sample t tests for differences between frequency bands: theta vs beta: $T_{199} = –41.02$, $P < 0.0001$; beta vs gamma: $T_{199} = 17.36$, $P < 0.0001$; gamma vs theta: $T_{199} = 37.10$, $P < 0.0001$.). This combined resampling analysis was designed to account for differences in numbers of correct and incorrect trials, which had the advantages of ensuring a balanced comparison across conditions and a robust number of incorrect trials. However, the contribution of individual subjects to the observed effects was unclear. To account for this, we quantified theta, beta and gamma responses for correct and incorrect trials separately, in each participant. Since some participants had no, or just a few, incorrect trials, we limited this analysis to include participants with more than 3 trials of each condition (resulting N = 5). Though numbers of incorrect trials were relatively low for some subjects, results of this analysis confirmed the combined findings: responses in all three frequencies were significantly above zero for correct trials (theta: $T_4 = 4.12$, $P = 0.014$; beta: $T_4 = 2.87$, $P = 0.045$; gamma: $T_4 = 4.71$, $P = 0.0092$), whereas only responses in theta band were significantly above zero for incorrect trials (theta: $T_4 = 7.28$, $P = 0.0019$; beta: $T_4 = 1.77$, $P = 0.15$; gamma: $T_4 = 1.41$, $P = 0.23$) (**Fig 4B**, lower right panels). These findings were also apparent in individual participant spectrograms (**S4 Fig 4B**).

373 Second, we looked for a relationship between task performance and responses in each
374 frequency band on a trial-by-trial basis. To account for differences within frequency
375 bands over time, we conducted this analysis during the inhale and exhale periods
376 separately. Trials were resampled to generate a distribution of correlation coefficients
377 representing the relationship between response amplitudes and behavioral accuracy for
378 each frequency band across the resampled trial sets. Significant correlations between
379 accuracy and amplitude were evident in the beta and gamma bands during both inhale
380 and exhale (50 bootstraps, t test against 0, FDR corrected threshold for significant
381 correlation coefficient; beta during inhale: $T_{49} = 31.25$, $P < 0.0001$; beta during exhale:
382 $T_{49} = 17.64$, $P < 0.0001$; gamma during inhale: $T_{49} = 23.70$, $P < 0.0001$; gamma during
383 exhale: $T_{49} = 28.25$, $P < 0.0001$.), but no such correlation was found in the theta band
384 (theta during inhale: $T_{49} = –2.04$, $P = 0.97$; theta during exhale: $T_{49} = –12.90$, $P = 1$). In
385 line with this, a direct statistical comparison across frequency bands showed that
386 correlations were significantly stronger between behavioral accuracy and amplitude for
387 beta and gamma bands compared to theta band during both inhale and exhale time
388 periods (**Fig 4C**) **(**two way repeated measures ANOVA: main effect of time window: $F_{1,}$
389 $_{49} = 111.08$, $P < 0.0001$; main effect of frequency band: $F_{2, 98} = 547.98$, $P < 0.0001$.
390 Paired sample t test across frequency bands during inhale for theta vs beta: $T_{49} = –$
391 29.37, $P < 0.0001$; for beta vs gamma: $T_{49} = 3.11$, $P = 0.0031$; for gamma vs theta: T_{49}
392 $= 24.95$, $P < 0.0001$; paired sample t test across frequency bands during exhale for
393 theta vs beta: $T_{49} = –26.51$, $P < 0.0001$; for beta vs gamma: $T_{49} = –11.13$, $P < 0.0001$;
394 for gamma vs theta: $T_{49} = 33.95$, $P < 0.0001$), also see **S4 Fig 4A**.

395 Finally, we used machine learning to perform a classification analysis on inhale and
396 exhale amplitudes for each frequency band, to determine whether these features could
397 predict task accuracy. To this end, we applied a binary linear support vector machine
398 (SVM) classifier to the bootstrapped data, plotted the receiver operative characteristic
399 (ROC) curves and calculated the area under curve (AUC), which was used together
400 with optimized classifier accuracy as the predictor of data separability. We found that
401 beta and gamma amplitudes were highly successful at separating the trials by accuracy,
402 while theta amplitudes were less so (**Fig 4D**). Specifically, gamma accuracy was
403 maximal at 91.5%, beta accuracy was also high at 91%, whereas theta accuracy was
404 lower, at 66.5%. This same procedure was applied to shuffled data, which resulted in
405 chance performance (accuracy = 52%), validating our methods. These findings
406 correspond well with the results from the two previous analyses, and, taken together,
407 suggest that beta and gamma band amplitudes are more strongly correlated with task
408 performance than theta amplitudes.

409 **Odor-elicited high-frequency oscillations are not driven by attention.**

410 Because the odor condition occurred during experimental trials and the no-odor
411 condition occurred between experimental trials, responses during the odor condition
412 could potentially have been impacted by attentional states that were not present during
413 the no-odor condition. Previous human and animal work suggests that olfactory cortical
414 responses are modulated by attention [95,96], particularly in lower frequency LFPs
415 [97,98]. To control for potential effects of attention on our findings, we analyzed
416 odorless sniffs taken in attended states during experimental trials. Each trial began with

417 a cue, followed by a delay (3–7s) prior to presentation of odor. Therefore, during many
418 trials, sniffs of clean air occurred between the cue and odor (**Fig 5A**). These sniffs
419 occurred during attended states, but did not contain odor, thus providing a means to
420 isolate the effects of attention from the effects of odor. Because a sniff did not always
421 occur between the cue and the odor, the number of trials in the attended odorless
422 condition was lower than the odor condition. Therefore, we resampled odor trials to
423 match the number across conditions. We computed spectrograms aligned to attended
424 odorless sniffs and compared them to those aligned to odor sniffs (**Fig 5B**, left and
425 middle). We found that attended odorless sniffs induced oscillations in low frequencies
426 (below 8 Hz) only ($P < 0.05$, FDR corrected), and found no stable higher frequency
427 oscillations (> 8Hz). We then computed the z-normalized difference across conditions
428 (**Fig 5B**, right) and found significant differences between attended odor trials and
429 attended no-odor trials in the theta, beta and gamma bands, such that oscillations in all
430 three frequency bands were increased when odor was present, even after removing the
431 effects of attention (**Fig 5B**, right; $P < 0.05$, FDR corrected). Since theta oscillations
432 were still detected in the attended no-odor condition, these findings suggest that the
433 increases in beta and gamma bands were independent of attention, whereas theta band
434 increases reflected, at least to some degree, attentional states.

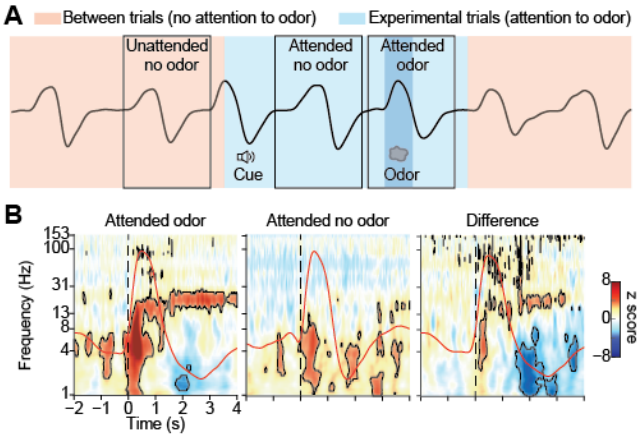

Fig 5. High frequency odor-elicited oscillations are not driven by attention. (A) Schematic illustration of attended and unattended conditions. Attended no-odor trials were defined as breaths taken during experimental trials, between the cue and the odor. No odor was present, but the participant was in an attended state. Blue area indicates the time of experimental trials, and pink areas indicates the time between trials. Black boxes indicate the analysis time windows for the different conditions. (B) Z-normalized spectrograms of attended odor and attended no-odor trials, and the difference between the two. Average respiratory signals are overlayed for each condition (red lines). Dashed line represents inhalation onset. Black contours indicate statistical significance (permutation tests as described elsewhere, $P < 0.05$, FDR corrected). The source data for panel (B) is available in S4 Data.

Low frequency phase modulates high frequency amplitude during inhale when odor is present.

Previous work suggests that odor-induced theta oscillations predict odor identities, even during a detection task that does not require participants to identify odors [57]. Here, we found that theta rhythms in our data appeared to have a relationship with beta responses, which appeared to oscillate at around 5 Hz during inhale. Specifically, the overall magnitude of beta oscillations increased and decreased rhythmically with a

453 frequency in the theta range, particularly in the first 1.5 to 2 seconds of the response
454 (**Fig 6A**, gray box). Based on this observation, we hypothesized that theta oscillations
455 might organize later-emerging higher frequency oscillations through phase modulation.
456 To estimate modulation of higher frequency amplitude by theta phase, we calculated the
457 modulation index (MI) [99] using theta phase as the modulating signal and a range of
458 high frequencies (13–150 Hz) as the amplitude signals, for both odor and no-odor
459 conditions (**Fig 6B**). We found that in the 1s time window following sniff onset, theta
460 phase significantly modulated beta and gamma oscillations during the odor condition (P
461 < 0.05, FDR corrected for MI in all frequency bands; peak MI at 16.16 Hz, mean z score
462 across all frequencies = 7.52), but not during the no-odor condition (mean z score
463 across all frequencies = 2.02).

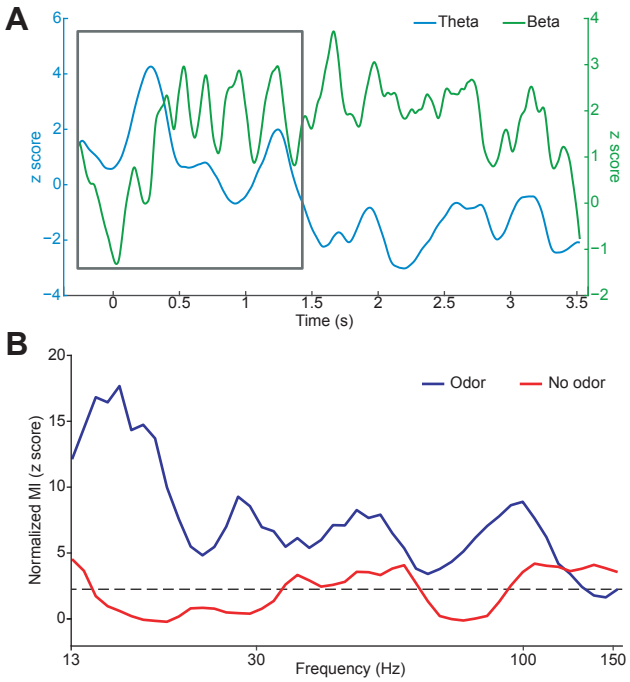

464

465 **Fig 6**. Theta phase modulates higher frequency amplitudes during inhale, when odor is present. (A)
466 Apparent rhythmic beta amplitude modulations at the theta frequency. With effects of attention subtracted
467 out, the average Z score of the amplitude of the odor responses over time is displayed for beta (green)

468 and theta (blue) frequency bands. The overall magnitude of beta oscillations increased and decreased
469 rhythmically with a frequency in the theta range, particularly in the first 1.5 to 2 seconds of the response
470 (gray box). (B) Phase-amplitude coupling between theta phase and higher frequency amplitudes. Z-
471 normalized modulation index (MI) of theta phase and higher frequency amplitudes (13 to 150 Hz), during
472 0–1s post sniff for all trials in the odor and no-odor conditions. Dashed line indicates FDR threshold for
473 significant MI ($P < 0.05$, FDR corrected). The source data for panel (A) and (B) are available in S4 Data.

474

475 Our phase-amplitude coupling analyses was performed during a window in which a
476 sensory-evoked potential could have occurred, and therefore the derived phase-
477 amplitude coupling could have been driven by the evoked potential having a steep
478 slope. To control for this possibility, we conducted a permutation analysis [100] in which
479 we shuffled the trial-by-trial relationship between theta phase and higher frequency
480 amplitude to test whether the modulation effect was due to the exact trial-by-trial
481 relationship or rather induced by a steep slope during each trial. We normalized the
482 observed MI to the trial-order-shuffled null distribution and still found significant effects
483 for the odor condition but not the no-odor condition (**S5 Fig 5**). This finding suggests
484 that higher frequency oscillations were modulated by theta phase during the early
485 period of sniffing, when theta amplitudes were significantly increased.

486

487 **Theta, beta and gamma oscillations are present across a range of olfactory tasks**
488 Studies in rodents suggest that different olfactory tasks may elicit distinct neural
489 oscillatory signatures [32,91]. Whether this is the case in the human olfactory system is
490 unknown. It is therefore possible that the oscillations we observed in the theta, beta and

491 gamma ranges were due to the nature of the olfactory task (identity matching to a cue,
492 as opposed to detection [57] or pure identification). To explore this possibility, we
493 present data from two additional subjects who performed 3 different olfactory tasks,
494 including a detection task, an edibility assessment task and an odor naming task. This
495 allowed us to determine if the nature of the task was the main driver of the effects we
496 observed, rather than the odors. None of the tasks involved matching to a previous cue.
497 For each task, trials began with a countdown to a cued sniff. Subjects self-initiated odor
498 delivery using a manual hand-held olfactometer that allowed for precise, sniff-controlled
499 timing of odor delivery. Following odor presentation, during the detection task, subjects
500 indicated whether or not they detected an odor via button press. During the edibility
501 assessment task, subjects indicated whether or not the odor was edible via button
502 press. During the naming task, subjects indicated whether or not they could name the
503 smell via button press, and then they spoke the name, if possible. All three of these
504 tasks resulted in highly similar oscillatory responses to odor in both subjects (**Fig 7**).
505 Both subjects, across all three task types, showed rapid increases in theta, followed by
506 oscillatory increases in beta and gamma that persisted into exhalation. Detailed
507 analyses of the responses to these different tasks is beyond the scope of this
508 manuscript; results are displayed here solely for the purpose of this control analysis,
509 which shows that the oscillations we observed in our original data set are present
510 across a range of olfactory tasks, and were therefore unlikely to have been driven solely
511 by the nature of the task.

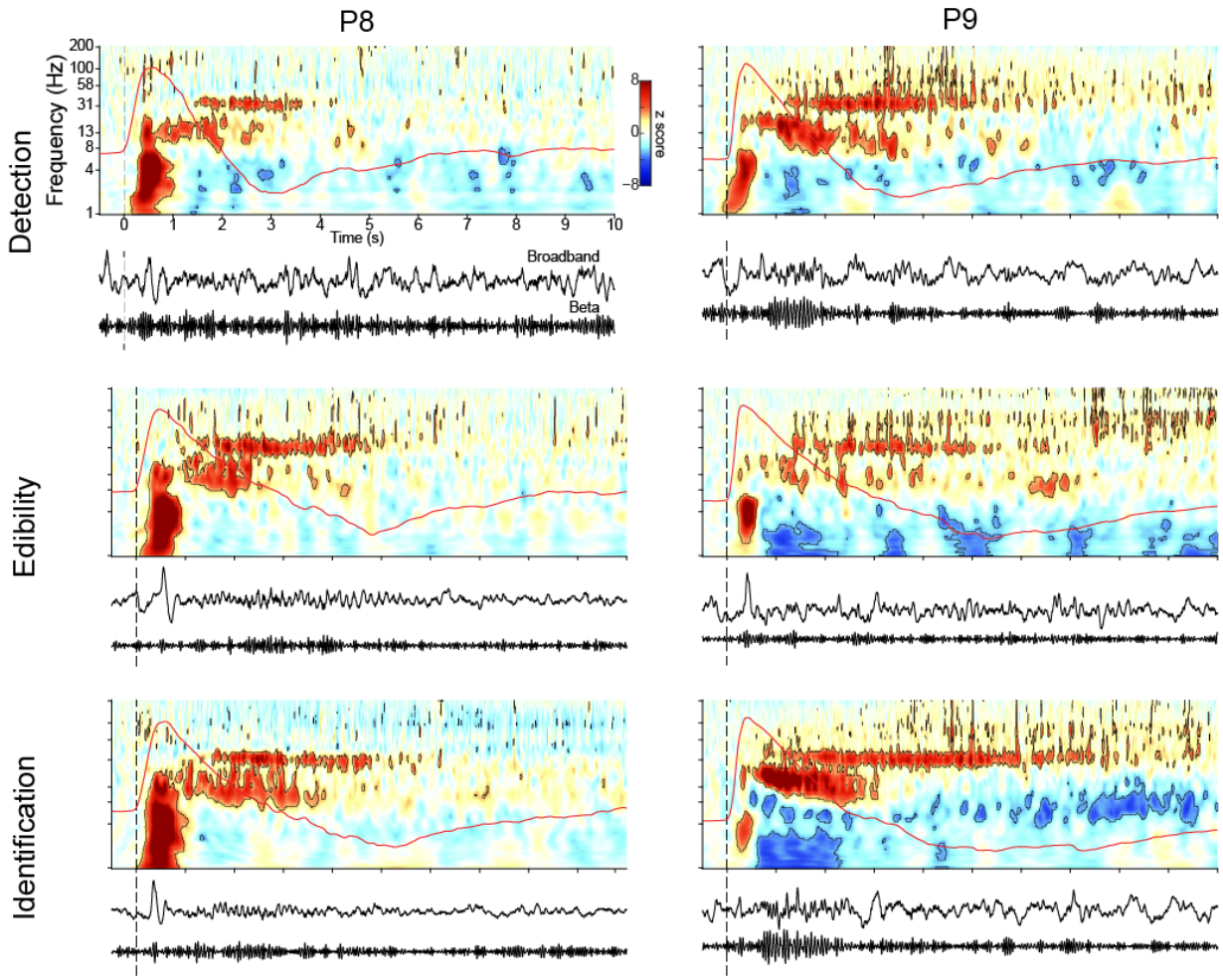

Fig 7. Odor-induced theta, beta and gamma oscillations are evident across a range of olfactory tasks. Shown are spectrograms from two participants (P8 and P9) who performed three different olfactory tasks including a detection task (top row), an edibility assessment task (middle row) and an odor naming task (bottom row). Short-dashed vertical line indicates sniff onsets. Average respiratory signals from each participant are shown as a red overlaid line on each spectrogram. Black contours indicate statistical significance ($P < 0.05$, FDR corrected). Below each panel is broad-band and beta-filtered time-series from one trial for that participant. The source data is available in S4 Data.

Discussion

522 We found that odor induces oscillations in human piriform cortex in the theta, beta and
523 gamma frequency bands, each with distinct temporal dynamics, forming the basis of a
524 characteristic human olfactory cortical response. While theta oscillations rapidly
525 emerged, peaked and dissipated within the first 500ms of inhalation, gamma and beta
526 oscillations emerged and peaked later, extending into the exhale period (see **Fig 2**, and
527 **Fig 3B and 3D**). These findings suggest that the spectrotemporal characteristics of
528 oscillations in piriform cortex in response to odor are similar in rodents and humans.
529 While our study cannot speak to the origin of these oscillations, it allows us to consider
530 the possibility that knowledge of the drivers of LFP oscillations in rodents [8] may be
531 applicable to humans, despite differences between species [101]; for example that beta
532 and gamma oscillations in piriform cortex rely on an intact olfactory tract from the bulb
533 [38], with important implications for our understanding of the top down or bottom up
534 nature of olfactory processing [102–104] . We further found that the strength of beta and
535 gamma oscillations was significantly more correlated with odor identification accuracy
536 than theta oscillations, suggesting beta and gamma rhythms are important for odor
537 identification in humans. Our work serves to unite results from previous intracranial
538 human studies that have reported odor-induced oscillations at both low and high
539 frequencies, with variable results [57,72–76,104].

540 Interestingly, we found that gamma rhythms were more tightly correlated to odor
541 identification accuracy than beta during exhale (see Fig 4C). Since gamma rhythms are
542 thought to reflect local computations [23,32,33,36,40,44,61,64], and beta oscillations
543 are thought to reflect long-range network interactions [27,30,35,36,61,64], local
544 computations in piriform cortex may have particular significance during exhale, though

545 our study does not directly address this and future studies on this topic are needed. Our
546 data also highlight an important role for theta oscillations in human piriform cortex, in
547 agreement with previous studies [57], as we found that theta phase modulated beta and
548 gamma amplitudes during inhalation, only when odor was present (see Fig 4). Rodent
549 work has identified functionally distinct subpopulations of piriform neurons that
550 differentially encode the intensity and identify of odor [82][81][105]. It is possible that the
551 distinct oscillations we identified in human piriform cortex represent distinct populations
552 of neurons that encode different features of the odor percept with unique temporal and
553 spectral properties, though future work is required to determine this. In particular, the
554 addition of single unit recordings may allow us to determine whether the different
555 oscillations are tied to different subpopulations of piriform neurons.

556 Theta, beta and gamma oscillations have been extensively studied in the olfactory
557 systems of rodents, providing insights into the functional roles of these oscillations in
558 olfactory perception [23,24,35–39,41,43,60,64,65,26,68,106,107,27–31,33,34].
559 Furthermore, an impactful body of rodent work has shown that the timing of olfactory
560 responses relative to sniffing behavior is an important mechanistic feature of odor
561 coding, enabling accurate olfactory percepts to form quickly [33,41,116,108–115].
562 Though much of this work has focused on the olfactory bulb, responses in rodent
563 piriform cortex also include temporal modulations [81,113,117], and its oscillations
564 reflect sniff phase [26,62,78]. In contrast to the extensive and elegant body of rodent
565 work, oscillations in human piriform cortex have been vastly understudied. Here,
566 dovetailing with animal work, we found that theta, beta and gamma oscillations emerged
567 at different times relative to sniff onset. The link between sniffing behavior and

oscillations in rodents, combined with dramatic differences in sniffing behavior between rodents and humans, raises some intriguing questions about the timing of odor responses in humans. When sampling odors, rodents engage in multiple sniffing strategies, and may sniff at rates up to 12 Hz [118–120]. Humans might at times increase their sniffing frequency a bit when smelling an odor, but often sample odors in a single sniff, and aren't able to reach sniffing frequencies of 12 Hz (though this has not yet been directly tested). Despite these large differences in sniffing behaviors across species, we found surprisingly similar time courses of odor responses in piriform cortex. For example, Frederick et al. [64] found that beta oscillations in rodent piriform cortex emerged at around 200 ms following odor onset, similar to our findings in human piriform cortex. We found that beta oscillations peaked and persisted longer than gamma oscillations, also in agreement with findings in rodents [59]. In rodents, the theta rhythm is actively shaped by sniffing behavior, which, in turn, shapes higher frequency oscillations. In humans, sniffing behavior almost never occurs at frequencies near the theta range, yet we found that theta oscillations shape higher frequency oscillations in the human olfactory system during inhalation, as is the case in rodents. This may suggest that the time scale of some odor-induced oscillations is not entirely dependent on breathing rate, and that network properties that support these rhythms may be conserved across species. Our findings support the idea that the theta rhythm serves as the "internal reference clock" of odor information processing [57], though future studies combining data from both humans and rodents, and potentially from noninvasive human olfactory bulb recordings [121] could contribute much-needed insights to answer this question.

591 An important consideration in comparing our findings to those in rodents is the nature of
592 the task. The two most commonly used olfactory tasks in rodent studies are the Go-No
593 Go (GNG) task and the 2-Alternative Forced Choice (2AFC) task [64,122–124]. The
594 GNG task requires a response only when a target odor is present, whereas the 2AFC
595 task requires a different response to each odor, depending on the identity of the odor.
596 Our task is more similar to the 2AFC task, as it requires subjects to respond differently
597 to each odor, depending on the identity of the odor. However, it is generally challenging
598 to compare tasks between species—both GNG and AFC tasks require training of
599 rodents, and include rewards during each trial. This is less common for human studies,
600 in which experimenters directly instruct subjects on the task, and rewards are not
601 required for subjects to learn the rules of the task. Several rodent studies have shown
602 differences in oscillatory signatures across different olfactory tasks and difficulty levels
603 [40,64]. It is therefore possible that differences in task-related responses could impact
604 differences between correct and incorrect trials between species [125–127]. A
605 worthwhile direction for future research includes a direct comparison between rodent
606 and human tasks, in which humans are trained and rewarded on a trial by trial basis,
607 exactly as is typically conducted with rodents.

608 We found that the magnitude of beta and gamma oscillations strongly predicted odor
609 identification accuracy, whereas this effect was weaker in the theta band, offering
610 support for distinct functional roles for the different rhythms in olfactory processing
611 [23,30,36,118]. Establishing beta rhythms in human piriform cortex may also lay the
612 groundwork for future work on olfactory networks and integration of olfactory information
613 with other cognitive processing streams and behaviors [30]. For example, integration of

614 olfactory information with language networks [128–130], memory networks [131–135],
615 sleep states [136–139], and other olfactory-guided behaviors [140,141] could potentially
616 involve interactions in beta oscillatory networks. Interestingly, we found that theta
617 oscillations, but not beta or gamma oscillations, increased during attended states when
618 no odor was present (**Fig 5B**), and prior to sniffing when odor was expected (**Fig 2A;**
619 **Fig 3A and 3D**). Taken together, these findings may indicate a role for theta in olfactory
620 attention, in line with previous studies suggesting that the phase and amplitude of lower
621 frequency oscillations reflect attentional states in the human brain [97]. Olfactory
622 attention also shapes neural responses in rodent olfactory cortex [95], and potential
623 future work may include a direct comparison of these oscillations between species. It
624 may also be interesting to explore these oscillations in other primary olfactory areas,
625 which may have similar neural responses to piriform cortex.

626 A limitation of our work is that we were unable to fully tease apart the contributions of
627 attention and expectation to our findings. Though we did conduct a control analysis
628 designed to look for effects of attention and anticipation by analyzing responses to sniffs
629 taken without anticipation of odor in between tasks, this analysis was limited by the fact
630 that there was no odor during the sniffs that we analyzed. A perfect control would
631 include presentation of odor in the absence of any expectation or anticipation. This
632 would be difficult to achieve, as multiple presentations of odor across an experimental
633 session almost undoubtedly would be anticipated after a couple of trials. This is an
634 interesting topic for future studies, once these challenging aspects of experimental
635 design are addressed.

636 Overall, our findings begin to define a characteristic human spectrotemporal odor
637 response, consisting of three distinct frequency bands with unique time courses relative
638 to sniff onset, with lower frequency phase modulating higher frequency amplitude, and
639 corresponding closely with cortical responses that have been found in rodents. This lays
640 the groundwork for future studies to further explore the functional role of the different
641 aspects of the human cortical olfactory response.

642 ## Methods

643 ### Ethics statement

644 This study was approved by the Institutional Review Board at Northwestern University,
645 under protocol #STU00201349, and the study adhered to the Declaration of Helsinki
646 and the Belmont Report. Participation was voluntary and written informed consent was
647 obtained from all participants.

648 ### Participants

649 Our study included iEEG data from nine patients with medication-resistant epilepsy. All
650 participants had depth electrodes implanted stereotactically for clinical pre-surgical
651 evaluation (**Fig 1A**). Electrode locations were determined solely based on clinical need
652 and, in our participant population, included piriform cortex within the medial temporal
653 lobe. Data were acquired at Northwestern Memorial Hospital.

654

655 ### Behavioral task

656 Participants performed a cued odor identification task in which they were asked whether
657 an odor matched a prior auditory cue. This task involved periodic presentation of odors
658 with inter-trial-intervals exceeding 6x the respiratory period of each individual, which
659 was at least 15 s for every participant. During this inter-trial period, participants breathed
660 naturally through the nose, and no odor was presented. The experimental trials were
661 conducted in each participant's hospital room, and were computer-controlled, presented
662 to participants using an Apple laptop computer running MATLAB (RRID: SCR_001622)
663 via the *PsychToolBox* extension (RRID: SCR_ 002881). Each trial of the task began
664 with an auditory cue consisting of either the word "rose" or the word "mint". The cue was
665 delivered by computer speaker. After a delay of 3 to 7 seconds, the odor of rose
666 (essential oil) or mint (methyl salicylate) was delivered through opaque squeeze bottles,
667 while nasal airflow was monitored in order to precisely determine sniff—and therefore
668 odor—onsets. We wanted participants to self-initiate odor delivery, so that they could
669 control the timing of the stimulus, and to ensure high quality data by allowing patients to
670 initiate trials at appropriate timing according to their individual situations. Note that this
671 design increased the jittered timing between the cue and the sniff, with patients initiating
672 the odor stimulus within 3 to 7 seconds following the cue. Participants were instructed
673 that following the auditory cue, when they were ready, they should exhale, bring the
674 bottle to their nose, and then sniff to sample the odor. For two patients, the
675 experimenter held the bottle and followed the same procedure. At the moment when the
676 patient sniffed, the experimenter sent a sync pulse to the clinical acquisition system via
677 button press. The experimenter's button press sent a signal via a data acquisition board
678 (USB-1208F, Measurement Computing), which translated TTL pulses from MATLAB

into the clinical EEG acquisition system (Nihon Kohden, Japan). Importantly, this button press did not provide sniff onset information—rather, it served to mark the odor-containing sniff in order to differentiate this sniff from other sniffs. Precise sniff onsets were determined by analysis of the nasal airflow signals, described in the methods. After smelling the odor, participants indicated whether the odor matched the cue via button press, with the exception of two patients who preferred to speak their response, which was recorded by an experimenter.

As previously described [98], participants completed between 48 and 64 trials, except for 1 participant who completed only 16 trials due to clinical constraints. The average inter-trial interval was 21.3 s, ranging from 14 to 28 s, across participants. The average performance on the task was 73.3% correct (P1: 79.69%, P2: 75.56%, P3: 31.25%, P4: 91.07%, P5: 100%, P6: 87.5%, P7: 46.88%), which means the response was “yes” when the odor matched with the sound cue or “no” when they were not matched. We found no difference in performance between the first (mean ± standard error: 73.98% ± 9.12%) and second (72.58% ± 10.72%) half of trials (two-tailed Wilcoxon signed-rank test; $z = 0.40$, $P = 0.69$). The performance was higher in cue-odor-matched trials (85% ± 7.08%) than nonmatched trials (58.17% ± 15.05%) (two-tailed Wilcoxon signed-rank test; $z = 2.20$, $P = 0.028$).

iEEG and respiratory signal recording

699 iEEG signals were recorded using the clinical EEG data acquisition system (Nihon
700 Kohden, Tokyo Japan) that is currently in use in Northwestern Memorial Hospital. The
701 sampling rate for each participant was determined clinically, and ranged from 500 to
702 2000 Hz across participants. The reference and ground consisted of an implanted
703 electrode strip on the surface of the brain facing the scalp. We recorded nasal airflow
704 using a piezoelectric pressure sensor (Salter Labs Model #5500) with a nasal cannula
705 placed at the patients' nostrils during the experiment. Nasal airflow signals were
706 recorded directly into the clinical acquisition system, and were therefore automatically
707 synchronized with the iEEG data. The signal was first mean centered, then key
708 respiratory features—including inhale and exhale onset, respiratory peak, and trough
709 volume and time—were detected automatically with MATLAB toolbox *BreathMetrics*,
710 developed by our lab [142], and then manually confirmed.

711 **Electrode Localization**

712 As previously described [97,98], to determine the implanted electrode locations, we
713 used pre-operative structural MRI scans and post-operative computed tomography (CT)
714 scans using the FMRIB Software Library's (FSL) registration tool *flirt* [143,144].
715 Individual CT images were registered to MRI images using 6 degrees of freedom and a
716 cost function of mutual information, which was followed by an affine registration with 12
717 degrees of freedom. Individual MRIs were registered to a standard Montreal
718 Neurological Institute (MNI) brain (MNI152_1mm_brain included in FSL) with 12
719 degrees of freedom. Finally, the transformation matrices generated above were

720 combined to create a transformation from the individual CT image to standard MNI
721 space.

722 The electrodes were localized by thresholding the raw CT image and calculating the un-
723 weighted mass center of each electrode. Finally, the coordinates were converted to
724 standard MNI space using the transformation matrix generated above.

725 Though we analyzed spectrograms from all electrodes on the PC depth wires and all
726 electrodes on the parietal grids, electrodes corresponding to those shown in Fig 2 were
727 selected by the following procedure. PC: For each subject, we first determined which
728 subset of electrodes was anatomically located inside PC using pre-drawn individual
729 ROIs based on the Human Brain Atlas [145]. This typically included between 1 and 3
730 electrodes. For the subjects who had only a single electrode in PC, we used that one.
731 For subjects with multiple electrodes within PC, we chose the one that was closest to
732 the center of PC. Notably, we also analyzed all piriform electrodes separately with
733 similar results.

734 **Time-frequency analysis**

735 For all time-frequency analyses, filtering was conducted using a two-pass, zero-phase-
736 lag, finite impulse response (FIR) filter, as implemented by the MATLAB toolbox *fieldtrip*
737 (RRID: SCR_004849), unless specified otherwise. We first low-pass filtered the iEEG
738 signal at 235 Hz and then removed 60 Hz noise and its harmonics with a band-stop filter
739 with a bandwidth of 4 Hz. We then downsampled the signal to 500Hz and re-referenced
740 the data to the common average. To compute spectrograms, we filtered the pre-

741 processed data between 1 to 200 Hz in 100 logarithmically increasing steps ranging
742 from 2 to 50 Hz in width. We kept only the first 95 frequency bands from 1 to 153 Hz as
743 our frequencies of interest for all subsequent analyses unless specified otherwise. The
744 analytical amplitudes of the filtered signals were calculated by taking the absolute value
745 of the Hilbert-transformed signal, and temporally smoothed with a moving average filter
746 kernel of 10 ms.

747 To compute spectrograms, we first created sniff-onset-aligned epochs, extending from –
748 2 s prior to 4 s following the sniff onset, for each trial. Sniff onsets were determined
749 using *BreathMetrics* [142]. Sniffs taken during experimental trials at the time of odor
750 presentation were used for the odor condition, sniffs taken in between trials when no
751 odor was present were used for the no-odor condition, and sniffs taken during
752 experimental trials in between the cue and odor were used for the attended-no-odor
753 condition. There were a larger number of no-odor trials compared to odor trials, and
754 therefore, no-odor trials were randomly sampled without replacement for each
755 participant separately to match trial numbers across conditions for further analysis. The
756 spectrograms were calculated by averaging the amplitude epochs across trials at each
757 frequency, which was further normalized by subtracting the baseline average. The time
758 window of [−0.55, −0.05] s prior to cue onset was used as baseline. To determine
759 statistical significance, we used a permutation method [97,98,146] to generate z score
760 values. For each repetition of the permutation process, the sniff onsets were circularly
761 shifted in time by a random amount while maintaining the relative distance between
762 them. Then, we calculate he average amplitude across these randomly shifted events.
763 The procedure above was repeated 10,000 times resulting a null distribution of baseline

764 amplitude. Finally, the baseline-corrected real spectrogram was divided by the standard
765 deviation of this null distribution, resulting a z score map. Raw power, baseline-
766 corrected power and z normalized maps can be seen in **S6 Fig 6**.

767 To compare the spectrograms between odor and no-odor condition, we used a
768 permutation method. In each permutation, the condition labels were shuffled across all
769 trials, and the difference of baseline-corrected spectrogram between permuted odor-
770 and no-odor-conditions were calculated. This process was repeated 10,000 times
771 resulting in a null distribution of spectrogram difference at each time-frequency point.
772 The mean and stand deviation of the null distribution was obtained using MATLAB's
773 *normfit* function. Finally, a z score of the real spectrogram difference was calculated by
774 subtracting the mean and then dividing by the stand deviation. The spectrograms
775 created for the attentional control analysis shown in Fig 4B were generated with the
776 same methods, with the number of trials adjusted to include equal numbers of odor and
777 attended-no-odor trials.

778 To compute the percentage change of the amplitude time series shown in **Fig 3A**, we
779 averaged the amplitude time series across frequencies within each of the following
780 frequency bands: theta 4–8 Hz, beta 13–30 Hz, and gamma 30–150 Hz, for each trial.
781 The percentage change of amplitude was calculated as (Amplitude-
782 Amplitude_baseline)/Amplitude_baseline for each trial. The baseline window was
783 defined as −500 ms to −50 ms relative to cue onset. To compare the percentage
784 change of amplitude between odor and no-odor conditions, we performed a paired

785 sample t test at each time point. Multiple comparisons across all time points were
786 corrected using FDR method.

787 In order to visualize the differences in temporal dynamics across frequency bands, we
788 created a z-normalized amplitude map for each frequency band using a bootstrapping
789 method (**Fig 3B**). First, each trial was baseline corrected and z-normalized. Then, in
790 each repetition, we resampled all 323 trials (with replacement), and calculated the
791 average across trials for each frequency band. A z-score matrix (repetition x time) was
792 generated for each frequency band after 2000 bootstraps (**Fig 3B**).

793

794 We then performed a cluster-based analysis to quantify the time course of significant
795 responses for each frequency band (**Fig 3C**). First, we performed a one sample t tests
796 against zero for z-normalized amplitudes for all trials at each time point for each
797 frequency band. To identify continuous significant clusters, We then used a cluster-
798 based statistical thresholding analysis to identify continuous significant clusters. The *P*
799 value threshold for initial clustering was set to $P = 0.01$, and the cluster size was defined
800 as the sum of the t-statistics of a given cluster. To generate a null distribution of the
801 cluster size, we used a permutation method. In each repetition (10000 repetition in
802 total), a random number of trials were circularly shifted separately, and the maximal
803 cluster size was calculated as described above. The 95th percentile of the distribution
804 was used as the cluster size significance threshold, which corresponds to cluster-based
805 corrected $P < 0.05$.

806 We next conducted an analysis to explore the timing and phase of responses in each
807 frequency band (**Fig 3D**). we calculated the distribution of respiratory phase values at
808 which the peak amplitude responses occurred using a bootstrapping method. For each
809 bootstrap, we resampled 323 trials (with replacement) while keeping the pairwise
810 relationship between LFP and breathing signals. The LFP and respiratory signals were
811 first averaged over resampled trials. To find the peaks of the LFP amplitude response,
812 we smoothed the amplitude time series using a moving average method with a kernel of
813 50 ms. Then, the respiratory phase of the maximal amplitude over the 4 s post-sniff time
814 period was extracted. The respiratory phase was obtained from the breathing signal
815 using Hilbert method. Finally, the distribution of the respiratory phases across trials
816 were qualified using PLV [147] as implemented in the MATLAB toolbox circstats (RRID:
817 SCR_016651) [148]. The Rayleigh test was performed to test for the non-uniformity of
818 phase distributions. For the peak timing analysis on the single participant level, we used
819 the same method.

820 We next conducted a series of analyses to look for relationships between LFPs and
821 odor identification accuracy (**Fig 4**). First, we computed amplitude spectrogram for odor
822 and no-odor conditions separately. The two spectrograms were z-normalized to the
823 same combined null distribution generated using methods described in the previous
824 section to rule out the effect of trial number difference across conditions. In order to
825 statistically compare the amplitude difference between correct and incorrect trials, we
826 conducted a resampling analysis. For each repetition, we resampled equal numbers of
827 correct and incorrect trials (71, with replacement) to ensure a fair comparison across
828 conditions. On each repetition, we calculated the mean of z-normalized amplitudes

829 across the entire time window for each frequency band for each condition (these
830 distributions are shown in **Fig 4B**), subtracted the mean of incorrect trials from the mean
831 of correct trials, and repeated this process 200 times to generate the distribution of
832 difference values between correct and incorrect trials. The difference values for each
833 frequency band was tested against 0 using one-sample t tests to generate statistics.
834 The distribution was plotted as scatter as well as box plot (**Fig 4B**).

835 We then conducted a bootstrap-correlation analysis to directly assess the correlation
836 between task performance and LFP amplitude of each frequency band for inhale and
837 exhale respectively on a trial-by-trial basis (**Fig 4C**). For each repetition (1000x) in the
838 analysis, we resampled 323 trials with replacement and calculated the accuracy of the
839 chosen trial set. We then calculated the mean amplitude during inhale and exhale
840 separately (inhale-exhale transition defined by phase angle of pi/2 for averaged
841 breathing signal) for all three frequency bands. We calculated Pearson's correlation
842 coefficients between task accuracy and mean amplitudes for inhale and exhale, for
843 each frequency band. We then repeated this entire process 50 times to generate a
844 distribution of correlation coefficient for each preparatory phase and frequency
845 condition. We used FDR to correct for multiple comparisons ($P < 0.05$) when we set the
846 significance threshold for the r value. We subsequently fisher-z-transformed all
847 Pearson's r values and conducted a repeated measures two-way ANOVA as well as
848 paired sample t tests to analyze the differences across frequency bands and respiratory
849 phases.

850 We next created scatter plot visualizations of amplitude responses during inhale and
851 exhale phases for correct and incorrect trials and fitted a linear SVM classifier to each of
852 the scatter plot in order to see how well the amplitude during inhale and exhale, taken
853 together, could predict task performance **(Fig 4D** and **4E).** To balance the discrepancy
854 between correct and incorrect trial numbers (252 vs. 71), we conducted a bootstrapping
855 analysis using equal numbers of trials across conditions on each repetition. For each
856 respiratory phase and frequency band, we sampled 30 trials within condition with
857 replacement each time, calculated percent change relative to baseline with the trial-wise
858 averaged amplitude time series, and calculated average amplitudes during inhale and
859 exhale for each trial set. Inhale and exhale periods were defined as 0–1.5s and 1.5–3 s
860 post sniff respectively for all trials. This process was repeated 500 times for both correct
861 and incorrect trials to generate a scatterplot of corresponding inhale and exhale
862 amplitudes for trials from both conditions. In order to test the separability of data, we
863 applied a linear binary SVM classifier using MATLAB function *fitcsvm* with five-fold
864 cross validation. ROC curves were generated using the function *perfcurve.*

865

866 **Phase-amplitude coupling analysis**

867 We calculated the modulation index (MI) to measure coupling between theta phase and
868 higher frequency amplitudes (13–150 Hz) (**Fig 5**). To do so, we extracted the phase
869 angle time series for the theta frequency band (4–8 Hz), and then from that phase time
870 series, created sniff-aligned trial epochs. Data from all trials was concatenated. To
871 generate the higher frequency amplitude data that was used to compute the MI, the raw

872 time series were filtered and amplitude-extracted (as described previously) to the same
873 47 log-spaced frequency bands (13.05–153.04 Hz), with logarithmically increasing
874 bandwidth, as described in the previous section for the time-frequency analysis. We
875 then concatenated this data identically to the theta phase data. MI was calculated as the
876 Kullbach-Leibner distance divided by the logged number of bins. To normalize the MI,
877 we created a null distribution of MI values using permutation method. For each
878 repetition, and for each frequency band, we circularly shifted the amplitude time series,
879 and calculated the MI between the shifted amplitudes and theta phase values. This
880 process was repeated 1000 times for each frequency band to generate the
881 corresponding null distribution of MI values. We then normalized the raw MI to the null
882 distributions to generate the z-scores, and FDR corrected the *P* values for multiple
883 comparisons. To control for the effect of evoked potential on phase-amplitude coupling,
884 we used a permutation method to ensure that the significant MI we observed was
885 unlikely due to steep slope of evoked potential occurring in every trial. For each
886 repetition, we shuffled the order of theta phase but kept the order of higher frequency
887 amplitude to randomize the trial-by-trial relationship, and calculated MI for each
888 frequency band based on the shuffled trials. This process was repeated 1000 times for
889 each frequency band to create a null distribution for the MI value under the null
890 hypothesis that the phase-amplitude coupling was due to steep waveform occurring in
891 every trial. We then normalized the raw MI to the null distributions to generate the z-
892 scores, and FDR corrected the *P* values for multiple comparisons.

893 **Control for nature of the task**

894 Two participants performed three different olfactory tasks over six separate blocks.
895 Patients performed two blocks of each task. The three tasks required the participant to
896 indicate: 1) whether or not they detected any odor (Detection task), 2) whether the odor
897 was edible (Edibility task), or 3) the identity of the odor (Naming task). For all three
898 tasks, each trial began with a countdown ("3, 2, 1, Sniff") which appeared in sequential
899 order, with each number lasting 1 s. The participant was instructed to sniff when the
900 word sniff appeared, using a manual hand-held olfactometer that allowed for sniff-
901 controlled timing of odor delivery. The hand-held olfactometer consisted of an odor
902 canister connected to a nose port, constructed with one-way valves at the outlet and
903 inlet such that the headspace was able to be sampled only and immediately upon
904 sniffing. The canister was contained inside of an opaque 3D printed case. Each run
905 consisted of 20 trials, resulting in 40 trials of each task type. Odors were of natural
906 origin, and included banana, salsa, liquid smoke, blood orange tea, peanut butter,
907 garlic, peppermint, pine and rose, for each trial. The tasks were performed while clinical
908 ongoing electrophysiological activity was recorded at a sampling rate of 1000 Hz using
909 a 256-channel clinical EEG acquisition system (Nihon Kohden). The respiratory signals
910 were recorded using a pressure sensor at the nose (Salter Labs). Time-frequency
911 analysis of odor-induced responses in the piriform cortex was conducted using the
912 methods described above.

913

914 **ACKNOWLEDGEMENTS**

We thank the patients and families of patients who volunteered to participate in this research; without their generous contributions of time and effort, this study would not have been possible. We thank Navid Shadlou for his technical expertise and support, and assistance with data collection. This work was supported by National Institutes of Health grants R01-DC016364 (NIDCD) and R01-DC018539 (NIDCD) to C. Z.

REFERENCES:

1. Başar E, Başar-Eroglu C, Karakaş S, Schürmann M. Gamma, alpha, delta, and theta oscillations govern cognitive processes. Int J Psychophysiol. 2001;39: 241–248. doi:10.1016/S0167-8760(00)00145-8
2. Buzsáki G. Theta oscillations in the hippocampus. Neuron. 2002;33: 325–340. doi:10.1016/S0896-6273(02)00586-X
3. Colgin LL, Denninger T, Fyhn M, Hafting T, Bonnevie T, Jensen O, et al. Frequency of gamma oscillations routes flow of information in the hippocampus. Nature. 2009;462: 353–357. doi:10.1038/nature08573
4. Engel AK, Fries P. Beta-band oscillations—signalling the status quo? Curr Opin Neurobiol. 2010;20: 156–165. doi:10.1016/j.conb.2010.02.015
5. Fontanini A, Bower JM. Slow-waves in the olfactory system: an olfactory perspective on cortical rhythms. Trends Neurosci. 2006;29: 429–437. doi:10.1016/j.tins.2006.06.013
6. Fröhlich F, McCormick DA. Endogenous electric fields may guide neocortical network activity. Neuron. 2010;67: 129–143. doi:10.1016/J.NEURON.2010.06.005

938 7. Heck DH, McAfee SS, Liu Y, Babajani-Feremi A, Rezaie R, Freeman WJ, et al.
939 Breathing as a fundamental rhythm of brain function. Front Neural Circuits.
940 2017;10: 115. doi:10.3389/fncir.2016.00115
941 8. Kay LM, Beshel J, Brea J, Martin C, Rojas-Líbano D, Kopell N. Olfactory
942 oscillations: the what, how and what for. Trends Neurosci. 2009;32: 207–214.
943 doi:10.1016/j.tins.2008.11.008
944 9. Lisman JE, Jensen O. The theta-gamma neural code. Neuron. 2013;77: 1002–
945 1016. doi:10.1016/j.neuron.2013.03.007
946 10. Murty DVPS, Shirhatti V, Ravishankar P, Ray S. Large visual stimuli induce two
947 distinct gamma oscillations in primate visual cortex. J Neurosci. 2018;38: 2730–
948 2744. doi:10.1523/JNEUROSCI.2270-17.2017
949 11. Zoefel B, VanRullen R. Oscillatory mechanisms of stimulus processing and
950 selection in the visual and auditory systems: state-of-the-art, speculations and
951 suggestions. Front Neurosci. 2017;11: 296. doi:10.3389/fnins.2017.00296
952 12. Deng Y, Choi I, Shinn-Cunningham B. Topographic specificity of alpha power
953 during auditory spatial attention. Neuroimage. 2020;207: 116360.
954 doi:10.1016/J.NEUROIMAGE.2019.116360
955 13. van Ede F, de Lange F, Jensen O, Maris E. Orienting attention to an upcoming
956 tactile event involves a spatially and temporally specific modulation of
957 sensorimotor alpha- and beta-band oscillations. J Neurosci. 2011;31: 2016–2024.
958 doi:10.1523/JNEUROSCI.5630-10.2011
959 14. Gross J, Schnitzler A, Timmermann L, Ploner M. Gamma oscillations in human
960 primary somatosensory cortex reflect pain perception. PLoS Biol. 2007;5: e133.

961 doi:10.1371/journal.pbio.0050133
962 15. Mayer A, Schwiedrzik CM, Wibral M, Singer W, Melloni L. Expecting to see a
963 letter: alpha oscillations as carriers of top-down sensory predictions. Cereb
964 Cortex. 2016;26: 3146–3160. doi:10.1093/CERCOR/BHV146
965 16. Todorovic A, van Ede F, Maris E, de Lange FP. Prior expectation mediates neural
966 adaptation to repeated sounds in the auditory cortex: an MEG study. J Neurosci.
967 2011;31: 9118–2913. doi:10.1523/JNEUROSCI.1425-11.2011
968 17. Adrian ED. Olfactory reactions in the brain of the hedgehog. J Physiol. 1942;100:
969 459–473. doi:10.1113/jphysiol.1942.sp003955
970 18. Barrie JM, Freeman WJ, Lenhart MD. Spatiotemporal analysis of prepyriform,
971 visual, auditory, and somesthetic surface EEGs in trained rabbits. J Neurophysiol.
972 1996;76: 520–539. doi:10.1152/jn.1996.76.1.520
973 19. Freeman WJ. A linear distributed feedback model for prepyriform cortex. Exp
974 Neurol. 1964;10: 525–547. doi:10.1016/0014-4886(64)90049-4
975 20. Freeman WJ. Phasic and long-term excitability changes in prepyriform cortex of
976 cats. Exp Neurol. 1962;5: 500–518. doi:10.1016/0014-4886(62)90059-6
977 21. Freeman WJ. Distribution in time and space of prepyriform electrical activity. J
978 Neurophysiol. 1959;22: 644–665. doi:10.1152/JN.1959.22.6.644
979 22. Freeman WJ. Measurement of oscillatory responses to electrical stimulation in
980 olfactory bulb of cat. J Neurophysiol. 1972;35: 762–779.
981 doi:10.1152/JN.1972.35.6.762
982 23. Beshel J, Kopell N, Kay LM. Olfactory bulb gamma oscillations are enhanced with
983 task demands. J Neurosci. 2007;27: 8358–8365. doi:10.1523/JNEUROSCI.1199-

984 07.2007
985 24. Chapuis J, Cohen Y, He X, Zhang Z, Jin S, Xu F, et al. Lateral entorhinal
986 modulation of piriform cortical activity and fine odor discrimination. J Neurosci.
987 2013;33: 13449–13459. doi:10.1523/JNEUROSCI.1387-13.2013
988 25. Cohen Y, Putrino D, Wilson DA. Dynamic cortical lateralization during olfactory
989 discrimination learning. J Physiol. 2015;593: 1701–1714.
990 doi:10.1113/jphysiol.2014.288381
991 26. Courtiol E, Buonviso N, Litaudon P. Odorant features differentially modulate
992 beta/gamma oscillatory patterns in anterior versus posterior piriform cortex.
993 Neuroscience. 2019;409: 26–34. doi:10.1016/j.neuroscience.2019.04.025
994 27. Gnaedinger A, Gurden H, Gourévitch B, Martin C. Multisensory learning between
995 odor and sound enhances beta oscillations. Sci Rep. 2019;9: 11236.
996 doi:10.1038/s41598-019-47503-y
997 28. Kay LM. Theta oscillations and sensorimotor performance. Proc Natl Acad Sci U
998 S A. 2005;102: 3863–3868. doi:10.1073/pnas.0407920102
999 29. Kay LM. Circuit oscillations in odor perception and memory. Prog Brain Res.
1000 2014;208: 223–251. doi:10.1016/B978-0-444-63350-7.00009-7
1001 30. Kay LM, Beshel J. A beta oscillation network in the rat olfactory system during a
1002 2-alternative choice odor discrimination task. J Neurophysiol. 2010;104: 829–839.
1003 doi:10.1152/jn.00166.2010
1004 31. Kay LM, Stopfer M. Information processing in the olfactory systems of insects and
1005 vertebrates. Semin Cell Dev Biol. 2006;17: 433–442.
1006 doi:10.1016/j.semcdb.2006.04.012

1007 32. Lepousez G, Lledo P-M. Odor discrimination requires proper olfactory fast
1008 oscillations in awake mice. Neuron. 2013;80: 1010–1024.
1009 doi:10.1016/j.neuron.2013.07.025
1010 33. Losacco J, Ramirez-Gordillo D, Gilmer J, Restrepo D. Learning improves
1011 decoding of odor identity with phase-referenced oscillations in the olfactory bulb.
1012 Elife. 2020;9: e52583. doi:10.7554/eLife.52583
1013 34. Lowry CA, Kay LM. Chemical factors determine olfactory system beta oscillations
1014 in waking rats. J Neurophysiol. 2007;98: 394–404. doi:10.1152/jn.00124.2007
1015 35. Martin C, Beshel J, Kay LM. An olfacto-hippocampal network is dynamically
1016 involved in odor-discrimination learning. J Neurophysiol. 2007;98: 2196–2205.
1017 doi:10.1152/jn.00524.2007
1018 36. Martin C, Ravel N. Beta and gamma oscillatory activities associated with olfactory
1019 memory tasks: different rhythms for different functional networks? Front Behav
1020 Neurosci. 2014;23: 218. doi:10.3389/fnbeh.2014.00218
1021 37. Mori K, Manabe H, Narikiyo K, Onisawa N. Olfactory consciousness and gamma
1022 oscillation couplings across the olfactory bulb, olfactory cortex, and orbitofrontal
1023 cortex. Front Psychol. 2013;4: 743. doi:10.3389/fpsyg.2013.00743
1024 38. Neville KR, Haberly LB. Beta and gamma oscillations in the olfactory system of
1025 the urethane-anesthetized rat. J Neurophysiol. 2003;90: 3921–3930.
1026 doi:10.1152/jn.00475.2003
1027 39. Poo C, Isaacson JS. Odor representations in olfactory cortex: “sparse” coding,
1028 global inhibition, and oscillations. Neuron. 2009;62: 850–861.
1029 doi:10.1016/j.neuron.2009.05.022

1030 40. Ravel N, Chabaud P, Martin C, Gaveau V, Hugues E, Tallon-Baudry C, et al.
1031 Olfactory learning modifies the expression of odour-induced oscillatory responses
1032 in the gamma (60-90 Hz) and beta (15-40 Hz) bands in the rat olfactory bulb. Eur
1033 J Neurosci. 2003;17: 350–358. doi:10.1046/j.1460-9568.2003.02445.x
1034 41. Rosero MA, Aylwin ML. Sniffing shapes the dynamics of olfactory bulb gamma
1035 oscillations in awake behaving rats. Eur J Neurosci. 2011;34: 787–799.
1036 doi:10.1111/J.1460-9568.2011.07800.X
1037 42. Wilson DA, Sullivan RM. Cortical processing of odor objects. Neuron. 2011;72:
1038 506–519. doi:10.1016/j.neuron.2011.10.027
1039 43. Zhou Y, Fang F-H, Pan P, Liu Z-R, Ji Y-H. Visual deprivation induce cross-modal
1040 enhancement of olfactory perception. Biochem Biophys Res Commun. 2017;486:
1041 833–838. doi:10.1016/j.bbrc.2017.03.140
1042 44. Buzsáki G, Wang X-J. Mechanisms of gamma oscillations. Annu Rev Neurosci.
1043 2012;35: 203–225. doi:10.1146/ANNUREV-NEURO-062111-150444
1044 45. Spencer KM, Niznikiewicz MA, Shenton ME, McCarley RW. Sensory-evoked
1045 gamma oscillations in chronic schizophrenia. Biol Psychiatry. 2008;63: 744–747.
1046 doi:10.1016/J.BIOPSYCH.2007.10.017
1047 46. Bartoli E, Bosking W, Foster BL. Seeing visual gamma oscillations in a new light.
1048 Trends Cogn Sci. 2020;24: 501–503. doi:10.1016/j.tics.2020.03.009
1049 47. Edden RAE, Muthukumaraswamy SD, Freeman TCA, Singh KD. Orientation
1050 discrimination performance is predicted by GABA concentration and gamma
1051 oscillation frequency in human primary visual cortex. J Neurosci. 2009;29: 15721–
1052 15726. doi:10.1523/JNEUROSCI.4426-09.2009

48. Hermes D, Miller KJ, Wandell BA, Winawer J. Stimulus dependence of gamma oscillations in human visual cortex. Cereb Cortex. 2015;25: 2951–2959. doi:10.1093/cercor/bhu091

49. Honkanen R, Rouhinen S, Wang SH, Palva JM, Palva S. Gamma oscillations underlie the maintenance of feature-specific information and the contents of visual working memory. Cereb Cortex. 2015;25: 3788–3801. doi:10.1093/CERCOR/BHU263

50. Muthukumaraswamy SD, Singh KD. Visual gamma oscillations: the effects of stimulus type, visual field coverage and stimulus motion on MEG and EEG recordings. Neuroimage. 2013;69: 223–230. doi:10.1016/J.NEUROIMAGE.2012.12.038

51. Bosman CA, Schoffelen JM, Brunet N, Oostenveld R, Bastos AM, Womelsdorf T, et al. Attentional stimulus selection through selective synchronization between monkey visual areas. Neuron. 2012;75: 875–888. doi:10.1016/J.NEURON.2012.06.037

52. Rodriguez E, George N, Lachaux J-PP, Martinerie J, Renault B, Varela FJ. Perception's shadow: long-distance synchronization of human brain activity. Nature. 1999;397: 430–433. doi:10.1038/17120

53. Samonds JM, Bonds AB. Gamma oscillation maintains stimulus structure-dependent synchronization in cat visual cortex. J Neurophysiol. 2005;93: 223–236. doi:10.1152/JN.00548.2004

54. Brosch M, Budinger E, Scheich H. Stimulus-related gamma oscillations in primate auditory cortex. J Neurophysiol. 2002;87: 2715–2725.

doi:10.1152/JN.2002.87.6.2715

55. Albouy P, Mattout J, Bouet R, Maby E, Sanchez G, Aguera P-E, et al. Impaired pitch perception and memory in congenital amusia: the deficit starts in the auditory cortex. Brain. 2013;136: 1639–1661. doi:10.1093/brain/awt082

56. Ross B, Tremblay KL, Alain C. Simultaneous EEG and MEG recordings reveal vocal pitch elicited cortical gamma oscillations in young and older adults. Neuroimage. 2020;204: 116253. doi:10.1016/j.neuroimage.2019.116253

57. Jiang H, Schuele S, Rosenow J, Zelano C, Parvizi J, Tao JX, et al. Theta oscillations rapidly convey odor-specific content in human piriform cortex. Neuron. 2017;94: 207-219.e4. doi:10.1016/j.neuron.2017.03.021

58. Cenier T, Amat C, Litaudon P, Garcia S, Lafaye de Micheaux P, Liquet B, et al. Odor vapor pressure and quality modulate local field potential oscillatory patterns in the olfactory bulb of the anesthetized rat. Eur J Neurosci. 2008;27: 1432–1440. doi:10.1111/j.1460-9568.2008.06123.x

59. David F, Courtiol E, Buonviso N, Fourcaud-Trocmé N. Competing mechanisms of gamma and beta oscillations in the olfactory bulb based on multimodal inhibition of mitral cells over a respiratory cycle. eNeuro. 2015;2: ENEURO.0018-15.2015. doi:10.1523/ENEURO.0018-15.2015

60. Fukunaga I, Herb JT, Kollo M, Boyden ES, Schaefer AT. Independent control of gamma and theta activity by distinct interneuron networks in the olfactory bulb. Nat Neurosci. 2014;17: 1208–1216. doi:10.1038/nn.3760

61. Kopell N, Ermentrout GB, Whittington MA, Traub RD. Gamma rhythms and beta rhythms have different synchronization properties. Proc Natl Acad Sci U S A.

1099 2000;97: 1867–1872. doi:10.1073/pnas.97.4.1867
1100 62. Litaudon P, Garcia S, Buonviso N. Strong coupling between pyramidal cell activity
1101 and network oscillations in the olfactory cortex. Neuroscience. 2008;156: 781–
1102 787. doi:10.1016/J.NEUROSCIENCE.2008.07.077
1103 63. Manabe H, Mori K. Sniff rhythm-paced fast and slow gamma-oscillations in the
1104 olfactory bulb: relation to tufted and mitral cells and behavioral states. J
1105 Neurophysiol. 2013;110: 1593–1599. doi:10.1152/jn.00379.2013
1106 64. Frederick DE, Brown A, Brim E, Mehta N, Vujovic M, Kay LM. Gamma and beta
1107 oscillations define a sequence of neurocognitive modes present in odor
1108 processing. J Neurosci. 2016;36: 7750–7767. doi:10.1523/JNEUROSCI.0569-
1109 16.2016
1110 65. Freeman WJ, Schneider W. Changes in spatial patterns of rabbit olfactory EEG
1111 with conditioning to odors. Psychophysiology. 1982;19: 44–56.
1112 doi:10.1111/J.1469-8986.1982.TB02598.X
1113 66. MacLeod K, Bäcker A, Laurent G. Who reads temporal information contained
1114 across synchronized and oscillatory spike trains? Nature. 1998;395: 693–698.
1115 doi:10.1038/27201
1116 67. Nusser Z, Kay LM, Laurent G, Homanics GE, Mody I. Disruption of GABAA
1117 receptors on GABAergic interneurons leads to increased oscillatory power in the
1118 olfactory bulb network. J Neurophysiol. 2001;86: 2823–2833.
1119 doi:10.1152/JN.2001.86.6.2823
1120 68. Stopfer M, Bhagavan S, Smith BH, Laurent G. Impaired odour discrimination on
1121 desynchronization of odour-encoding neural assemblies. Nature. 1997;390: 70–

74. doi:10.1038/36335

69. Viana Di Prisco G, Freeman WJ. Odor-related bulbar EEG spatial pattern analysis during appetitive conditioning in rabbits. Behav Neurosci. 1985;99: 964–978. doi:10.1037/0735-7044.99.5.964

70. Rojas-Líbano D, Frederick DE, Egaña J, Kay LM. The olfactory bulb theta rhythm follows all frequencies of diaphragmatic respiration in the freely behaving rat. Front Behav Neurosci. 2014;8: 214. doi:10.3389/fnbeh.2014.00214

71. Xu W, Wilson DA. Odor-evoked activity in the mouse lateral entorhinal cortex. Neuroscience. 2012;223: 12–20. doi:10.1016/j.neuroscience.2012.07.067

72. Hudry J, Ryvlin P, Royet J-P, Mauguière F. Odorants elicit evoked potentials in the human amygdala. Cereb Cortex. 2001;11: 619–627. doi:10.1093/CERCOR/11.7.619

73. Jung J, Hudry J, Ryvlin P, Royet J-P, Bertrand O, Lachaux J-P. Functional significance of olfactory-induced oscillations in the human amygdala. Cereb Cortex. 2006;16: 1–8. doi:10.1093/cercor/bhi090

74. Hughes JR, Andy OJ. The human amygdala. I. Electrophysiological responses to odorants. Electroencephalogr Clin Neurophysiol. 1979;46: 428–443. doi:10.1016/0013-4694(79)90144-5

75. Hughes JR, Hendrix DE, Wetzel N, Johnston JW. Correlations between electrophysiological activity from the human olfactory bulb and the subjective response to odoriferous stimuli. Electroencephalogr Clin Neurophysiol. 1970;28: 97–8. Available: http://www.ncbi.nlm.nih.gov/pubmed/4188883

76. Hudry J. Olfactory short-term memory and related amygdala recordings in

1145 patients with temporal lobe epilepsy. Brain. 2003;126: 1851–1863.
1146 doi:10.1093/brain/awg192
1147 77. Buonviso N, Amat C, Litaudon P, Roux S, Royet J-P, Farget V, et al. Rhythm
1148 sequence through the olfactory bulb layers during the time window of a respiratory
1149 cycle. Eur J Neurosci. 2003;17: 1811–1819. doi:10.1046/j.1460-
1150 9568.2003.02619.x
1151 78. Herrero JL, Khuvis S, Yeagle E, Cerf M, Mehta AD. Breathing above the brain
1152 stem: volitional control and attentional modulation in humans. J Neurophysiol.
1153 2018;119: 145–159. doi:10.1152/jn.00551.2017
1154 79. Lockmann AL V., Laplagne DA, Tort ABL. Olfactory bulb drives respiration-
1155 coupled beta oscillations in the rat hippocampus. Eur J Neurosci. 2018;48: 2663–
1156 2673. doi:10.1111/ejn.13665
1157 80. Pashkovski SL, Iurilli G, Brann D, Chicharro D, Drummey K, Franks K, et al.
1158 Structure and flexibility in cortical representations of odour space. Nature.
1159 2020;583: 253–258. doi:10.1038/s41586-020-2451-1
1160 81. Bolding KA, Franks KM. Complementary codes for odor identity and intensity in
1161 olfactory cortex. Elife. 2017;6: pii: e22630. doi:10.7554/eLife.22630
1162 82. Roland B, Deneux T, Franks KM, Bathellier B, Fleischmann A. Odor identity
1163 coding by distributed ensembles of neurons in the mouse olfactory cortex. Elife.
1164 2017;6: e26337. doi:10.7554/eLife.26337
1165 83. Sobel N, Prabhakaran V, Desmond JE, Glover GH, Goode RL, Sullivan E V, et al.
1166 Sniffing and smelling: separate subsystems in the human olfactory cortex. Nature.
1167 1998;392: 282–286. doi:10.1038/32654

1168 84. Mainland J, Sobel N. The sniff is part of the olfactory percept. Chem Senses.
1169 2006;31: 181–196. doi:10.1093/chemse/bjj012
1170 85. Zelano C, Jiang H, Zhou G, Arora N, Schuele S, Rosenow J, et al. Nasal
1171 respiration entrains human limbic oscillations and modulates cognitive function. J
1172 Neurosci. 2016;36: 12448–12467. doi:10.1523/JNEUROSCI.2586-16.2016
1173 86. Kalcher J, Pfurtscheller G. Discrimination between phase-locked and non-phase-
1174 locked event-related EEG activity. Electroencephalogr Clin Neurophysiol.
1175 1995;94: 381–384. doi:10.1016/0013-4694(95)00040-6
1176 87. Donner TH, Siegel M. A framework for local cortical oscillation patterns. Trends
1177 Cogn Sci. 2011;15: 191–199. doi:10.1016/j.tics.2011.03.007
1178 88. Cohen MX. Differences among total, phase-locked, and non-phase-locked power
1179 and intertrial phase consistency. Analyzing neural time series data.
1180 Massachusetts Institute of Technology; 2014. pp. 259–262.
1181 89. Pfurtscheller G, Lopes Da Silva FH. Event-related EEG/MEG synchronization and
1182 desynchronization: basic principles. Clin Neurophysiol. 1999;110: 1842–1857.
1183 doi:10.1016/S1388-2457(99)00141-8
1184 90. Tallon-Baudry C, Bertrand O. Oscillatory gamma activity in humans and its role in
1185 object representation. Trends Cogn Sci. 1999;3: 151–162. doi:10.1016/S1364-
1186 6613(99)01299-1
1187 91. Barnes DC, Chapuis J, Chaudhury D, Wilson DA. Odor fear conditioning modifies
1188 piriform cortex local rield potentials both during conditioning and during post-
1189 conditioning sleep. PLoS One. 2011;6: e18130.
1190 doi:10.1371/journal.pone.0018130

92. van der Meer M. Integrating early results on ventral striatal gamma oscillations in the rat. Front Neurosci. 2010;0: 300. doi:10.3389/fnins.2010.00300

93. Bressler SL, Freeman WJ. Frequency analysis of olfactory system EEG in cat, rabbit, and rat. Electroencephalogr Clin Neurophysiol. 1980;50: 19–24. doi:10.1016/0013-4694(80)90319-3

94. Rojas-Líbano D, Kay LM. Olfactory system gamma oscillations: the physiological dissection of a cognitive neural system. Cogn Neurodyn. 2008;2: 179–194. doi:10.1007/s11571-008-9053-1

95. Carlson KS, Gadziola MA, Dauster ES, Wesson DW. Selective attention controls olfactory decisions and the neural encoding of odors. Curr Biol. 2018;28: 2195-2205.e4. doi:10.1016/j.cub.2018.05.011

96. Zelano C, Bensafi M, Porter J, Mainland J, Johnson B, Bremner E, et al. Attentional modulation in human primary olfactory cortex. Nat Neurosci. 2005;8: 114–120. doi:10.1038/nn1368

97. Arabkheradmand G, Zhou G, Noto T, Yang Q, Schuele SU, Parvizi J, et al. Anticipation-induced delta phase reset improves human olfactory perception. Hanslmayr S, editor. PLOS Biol. 2020;18: e3000724. doi:10.1371/journal.pbio.3000724

98. Zhou G, Lane G, Noto T, Arabkheradmand G, Gottfried JA, Schuele SU, et al. Human olfactory-auditory integration requires phase synchrony between sensory cortices. Nat Commun. 2019;10: 1168. doi:10.1038/s41467-019-09091-3

99. Tort ABL, Komorowski R, Eichenbaum H, Kopell N. Measuring phase-amplitude coupling between neuronal oscillations of different frequencies. J Neurophysiol.

1214 2010;104: 1195–210. doi:10.1152/jn.00106.2010
1215 100. Voytek B, D'Esposito M, Crone N, Knight RT. A method for event-related
1216 phase/amplitude coupling. Neuroimage. 2013;64: 416–424.
1217 doi:10.1016/j.neuroimage.2012.09.023
1218 101. Lane G, Zhou G, Noto T, Zelano C. Assessment of direct knowledge of the
1219 human olfactory system. Exp Neurol. 2020;329: 113304.
1220 doi:10.1016/j.expneurol.2020.113304
1221 102. Olofsson JK, Bowman NE, Khatibi K, Gottfried JA. A time-based account of the
1222 perception of odor objects and valences. Psychol Sci. 2012;23: 1224–1232.
1223 doi:10.1177/0956797612441951
1224 103. Singh AK, Touhara K, Okamoto M. Electrophysiological correlates of top-down
1225 attentional modulation in olfaction. Sci Rep. 2019;9: 4953. doi:10.1038/s41598-
1226 019-41319-6
1227 104. Iravani B, Arshamian A, Lundqvist M, Kay LM, Wilson DA, Lundström JN. Odor
1228 identity can be extracted from the reciprocal connectivity between olfactory bulb
1229 and piriform cortex in humans. Neuroimage. 2021;237: 118130.
1230 doi:10.1016/J.NEUROIMAGE.2021.118130
1231 105. Xia CZ, Adjei S, Wesson DW. Coding of odor stimulus features among secondary
1232 olfactory structures. J Neurophysiol. 2015;114: 736–745.
1233 doi:10.1152/JN.00902.2014/ASSET/IMAGES/LARGE/Z9K0121531780004.JPEG
1234 106. Ketchum K, Haberly L. Synaptic events that generate fast oscillations in piriform
1235 cortex. J Neurosci. 1993;13: 3980–3985. doi:10.1523/JNEUROSCI.13-09-
1236 03980.1993

1237 107. Kay LM, Freeman WJ. Bidirectional processing in the olfactory-limbic axis during
1238 olfactory behavior. Behav Neurosci. 1998;112: 541–553. doi:10.1037/0735-
1239 7044.112.3.541
1240 108. Bathellier B, Buhl DL, Accolla R, Carleton A. Dynamic ensemble odor coding in
1241 the mammalian olfactory bulb: sensory information at different timescales.
1242 Neuron. 2008;57: 586–598. doi:10.1016/j.neuron.2008.02.011
1243 109. Blauvelt DG, Sato TF, Wienisch M, Murthy VN. Distinct spatiotemporal activity in
1244 principal neurons of the mouse olfactory bulb in anesthetized and awake states.
1245 Front Neural Circuits. 2013;7: 46. doi:10.3389/fncir.2013.00046
1246 110. Kepecs A, Uchida N, Mainen ZF. The sniff as a unit of olfactory processing. Chem
1247 Senses. 2006;31: 167–179. doi:10.1093/chemse/bjj016
1248 111. Phillips ME, Sachdev RNS, Willhite DC, Shepherd GM. Respiration drives
1249 network activity and modulates synaptic and circuit processing of lateral inhibition
1250 in the olfactory bulb. J Neurosci. 2012;32: 85–98. doi:10.1523/JNEUROSCI.4278-
1251 11.2012
1252 112. Grosmaitre X, Santarelli L, Tan J, Luo M, Ma M. Dual functions of mammalian
1253 olfactory sensory neurons as odor detectors and mechanical sensors. Nat
1254 Neurosci. 2007;10: 348–354. doi:10.1038/NN1856
1255 113. Rennaker RL, Chen C-FF, Ruyle AM, Sloan AM, Wilson DA. Spatial and temporal
1256 distribution of odorant-evoked activity in the piriform cortex. J Neurosci. 2007;27:
1257 1534–1542. doi:10.1523/jneurosci.4072-06.2007
1258 114. Shusterman R, Smear MC, Koulakov AA, Rinberg D. Precise olfactory responses
1259 tile the sniff cycle. Nat Neurosci. 2011;14: 1039–1044. doi:10.1038/nn.2877

1260 115. Uchida N, Kepecs A, Mainen ZF. Seeing at a glance, smelling in a whiff: rapid
1261 forms of perceptual decision making. Nat Rev Neurosci. 2006;7: 485–491.
1262 doi:10.1038/nrn1933
1263 116. Verhagen J V, Wesson DW, Netoff TI, White JA, Wachowiak M. Sniffing controls
1264 an adaptive filter of sensory input to the olfactory bulb. Nat Neurosci. 2007;10:
1265 631–639. doi:10.1038/nn1892
1266 117. Haddad R, Lanjuin A, Madisen L, Zeng H, Murthy VNN, Uchida N. Olfactory
1267 cortical neurons read out a relative time code in the olfactory bulb. Nat Neurosci.
1268 2013;16: 949–957. doi:10.1038/nn.3407
1269 118. Frederick DE, Brown A, Tacopina S, Mehta N, Vujovic M, Brim E, et al. Task-
1270 dependent behavioral dynamics make the case for temporal integration in multiple
1271 strategies during odor processing. J Neurosci. 2017;37: 4416–4426.
1272 doi:10.1523/JNEUROSCI.1797-16.2017
1273 119. Kepecs A, Uchida N, Mainen ZF. Rapid and precise control of sniffing during
1274 olfactory discrimination in rats. J Neurophysiol. 2007;98: 205–213.
1275 doi:10.1152/jn.00071.2007
1276 120. Sirotin YB, Costa ME, Laplagne DA. Rodent ultrasonic vocalizations are bound to
1277 active sniffing behavior. Front Behav Neurosci. 2014;8: 399.
1278 doi:10.3389/FNBEH.2014.00399
1279 121. Iravani B, Arshamian A, Ohla K, Wilson DA, Lundström JN. Non-invasive
1280 recording from the human olfactory bulb. Nat Commun. 2020;11: 648.
1281 doi:10.1038/s41467-020-14520-9
1282 122. Kay LM, Beshel J, Martin C. When good enough is best. Neuron. 2006;51: 277–

1283 278. doi:10.1016/J.NEURON.2006.07.015
1284 123. Friedrich RW. Mechanisms of odor discrimination: neurophysiological and
1285 behavioral approaches. Trends Neurosci. 2006;29: 40–47.
1286 doi:10.1016/J.TINS.2005.10.004
1287 124. Frederick DE, Rojas-Líbano D, Scott M, Kay LM. Rat behavior in Go/No-Go and
1288 two-alternative choice odor discrimination: differences and similarities. Behav
1289 Neurosci. 2011;125: 588–603. doi:10.1037/A0024371
1290 125. Kay LM, Laurent G. Odor- and context-dependent modulation of mitral cell activity
1291 in behaving rats. Nat Neurosci. 1999;2: 1003–1009. doi:10.1038/14801
1292 126. Doucette W, Restrepo D. Profound context-dependent plasticity of mitral cell
1293 responses in olfactory bulb. PLOS Biol. 2008;6: e258.
1294 doi:10.1371/JOURNAL.PBIO.0060258
1295 127. Doucette W, Gire DH, Whitesell J, Carmean V, Lucero MT, Restrepo D.
1296 Associative cortex features in the first olfactory brain relay station. Neuron.
1297 2011;69: 1176–1187. doi:10.1016/J.NEURON.2011.02.024
1298 128. Majid A. Human olfaction at the intersection of language, culture, and biology.
1299 Trends Cogn Sci. 2021;25: 111–123. doi:10.1016/j.tics.2020.11.005
1300 129. Majid A, Kruspe N. Hunter-gatherer olfaction is special. Curr Biol. 2018;28: 409-
1301 413.e2. doi:10.1016/J.CUB.2017.12.014
1302 130. Olofsson JK, Gottfried JA. The muted sense: neurocognitive limitations of
1303 olfactory language. Trends Cogn Sci. 2015;19: 314–321.
1304 doi:10.1016/j.tics.2015.04.007
1305 131. Arshamian A, Iravani B, Majid A, Lundström JN. Respiration modulates olfactory

1306 memory consolidation in humans. J Neurosci. 2018;38: 10286–10294.
1307 doi:10.1523/JNEUROSCI.3360-17.2018
1308 132. Arzi A, Rozenkrantz L, Holtzman Y, Secundo L, Sobel N. Sniffing patterns
1309 uncover implicit memory for undetected odors. Curr Biol. 2014;24: R263–R264.
1310 doi:10.1016/j.cub.2014.02.004
1311 133. Wilson DA, Stevenson RJ. The fundamental role of memory in olfactory
1312 perception. Trends Neurosci. 2003;26: 243–247. doi:10.1016/S0166-
1313 2236(03)00076-6
1314 134. Yeshurun Y, Lapid H, Dudai Y, Sobel N. The privileged brain representation of
1315 first olfactory associations. Curr Biol. 2009;19: 1869–1874.
1316 doi:10.1016/j.cub.2009.09.066
1317 135. Zhou G, Olofsson JK, Koubeissi MZ, Menelaou G, Rosenow J, Schuele SU, et al.
1318 Human hippocampal connectivity is stronger in olfaction than other sensory
1319 systems. Prog Neurobiol. 2021;201: 102027.
1320 doi:10.1016/j.pneurobio.2021.102027
1321 136. Arzi A, Sela L, Green A, Givaty G, Dagan Y, Sobel N. The influence of odorants
1322 on respiratory patterns in sleep. Chem Senses. 2010;35: 31–40.
1323 doi:10.1093/chemse/bjp079
1324 137. Hauner KK, Howard JD, Zelano C, Gottfried JA. Stimulus-specific enhancement
1325 of fear extinction during slow-wave sleep. Nat Neurosci. 2013;16: 1553–1555.
1326 doi:10.1038/nn.3527
1327 138. Perl O, Arzi A, Sela L, Secundo L, Holtzman Y, Samnon P, et al. Odors enhance
1328 slow-wave activity in non-rapid eye movement sleep. J Neurophysiol. 2016;115:

2294–2302. doi:10.1152/JN.01001.2015

139. Rasch B, Buchel C, Gais S, Born J. Odor cues during slow-wave sleep prompt declarative memory consolidation. Science (80-). 2007;315: 1426–1429. doi:10.1126/science.1138581

140. Bhutani S, Howard JD, Reynolds R, Zee PC, Gottfried J. Olfactory connectivity mediates sleep-dependent food choices in humans. Elife. 2019;8: e49053. doi:10.7554/ELIFE.49053

141. Howard JD, Reynolds R, Smith DE, Voss JL, Schoenbaum G, Kahnt T. Targeted stimulation of human orbitofrontal networks disrupts outcome-guided behavior. Curr Biol. 2020;30: 490-498.e4. doi:10.1016/J.CUB.2019.12.007

142. Noto T, Zhou G, Schuele S, Templer J, Zelano C. Automated analysis of breathing waveforms using BreathMetrics: a respiratory signal processing toolbox. Chem Senses. 2018;43: 583–597. doi:10.1093/chemse/bjy045

143. Jenkinson M, Smith S. A global optimisation method for robust affine registration of brain images. Med Image Anal. 2001;5: 143–156. doi:10.1016/S1361-8415(01)00036-6

144. Jenkinson M, Bannister P, Brady M, Smith S. Improved optimization for the robust and accurate linear registration and motion correction of brain images. Neuroimage. 2002;17: 825–841. doi:10.1006/nimg.2002.1132

145. Mai JK, Majtanik M, Paxinos G. Atlas of the human brain. 4th ed. New York: Academic Press; 2015.

146. Canolty RT. Spatiotemporal dynamics of word processing in the human brain. Front Neurosci. 2007;1: 185–196. doi:10.3389/neuro.01.1.1.014.2007

147. Aydore S, Pantazis D, Leahy RM. A note on the phase locking value and its properties. Neuroimage. 2013;74: 231–244. doi:10.1016/j.neuroimage.2013.02.008

148. Berens P. CircStat : a MATLAB toolbox for circular statistics. J Stat Softw. 2009;31: 1–21. doi:10.18637/jss.v031.i10

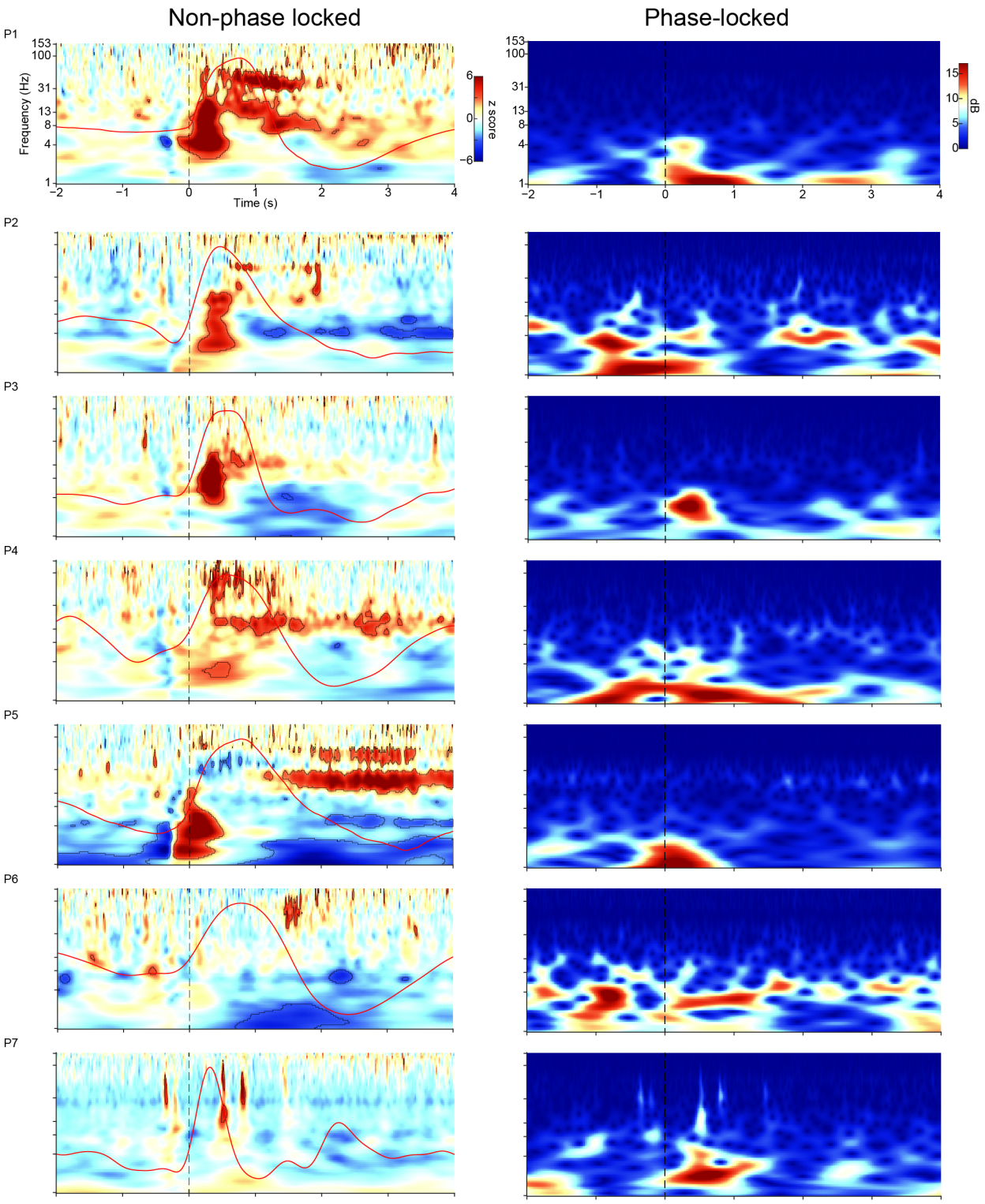
Non-phase locked
Phase-locked
P1
P2
P3
P4
P5
P6
P7
Frequency (Hz)
Time (s)
z score
dB

1361

1362 S1 Fig. Related to Fig 2. Odor-induced and odor-evoked spectrograms. Non-phase-
1363 locked (left) and phase-locked (right) spectrograms are shown for each participant (P1–
1364 P7). The non-phase-locked spectrogram was obtained by subtracting the event-related
1365 potential from each trial before time-frequency decomposition. The red solid overlay
1366 indicates each participant's respiratory signal. Black outlines indicate statistically
1367 significant clusters ($P < 0.05$, false-discovery-rate corrected). The phase-locked
1368 spectrogram was calculated as the baseline-corrected time-frequency decomposition of
1369 the event-related potential. The vertical short-dashed lines indicate sniff onset. The
1370 source is available in S5 Data.

1371

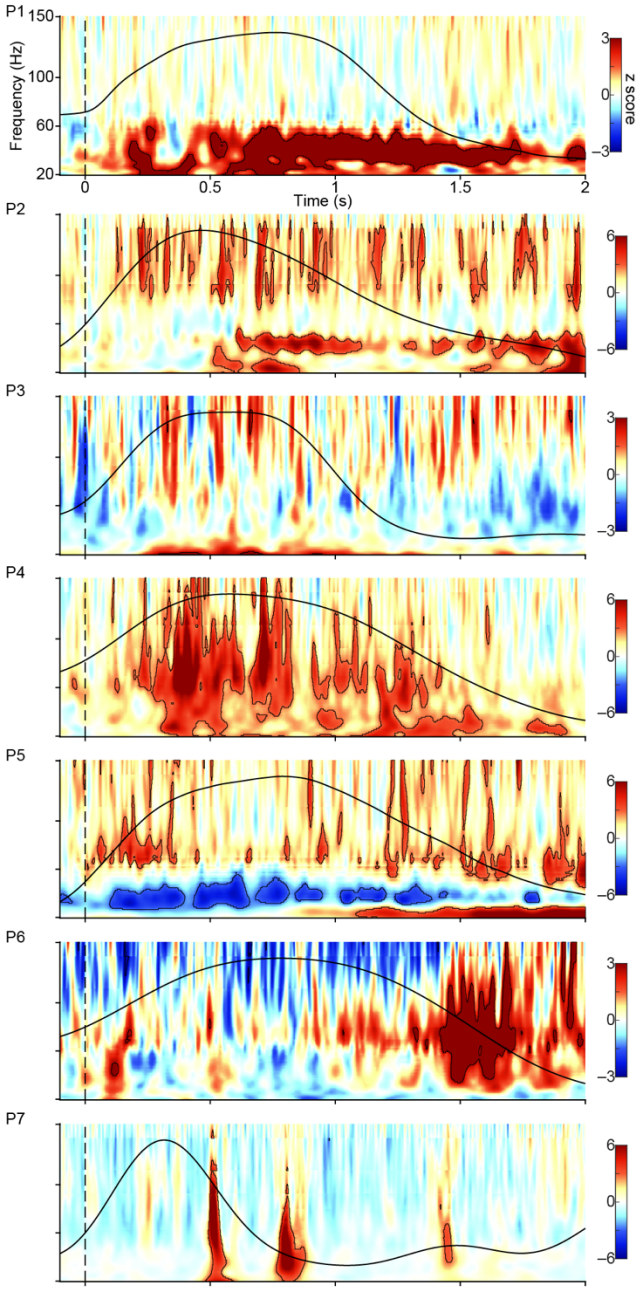

S2 Fig. Related to Fig 2. Sniff-onset aligned spectrograms with linear frequency scale. The black solid overlay indicates each participant's (P1–P7) respiratory signal. Black outlines indicate statistically significant clusters ($P < 0.05$, false-discovery-rate corrected). The vertical short-dashed line indicates sniff onset. The source is available in S5 Data.

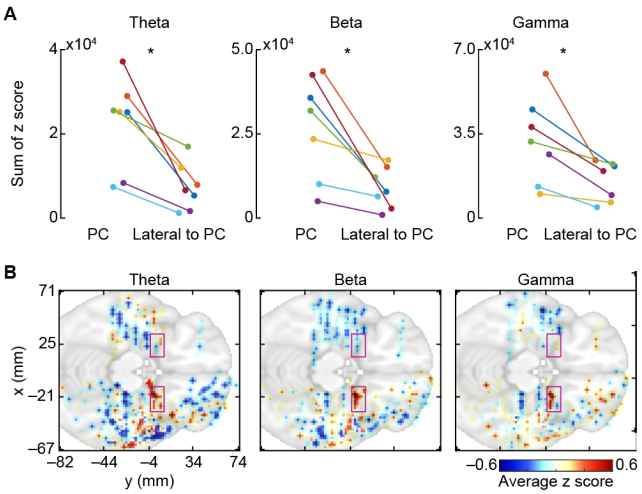

S3 Fig. Related to Fig 2. Odor-induced responses are maximal in piriform cortex. (A) Odor-induced amplitude (sum of z score) is larger in the depth wire located in the piriform cortex (PC) compared to those located outside of the piriform cortex (Lateral to PC) in theta, beta and gamma frequency bands. * indicates statistically significant difference (two-tailed paired t test). (B) The mean z score was calculated over a time window of 2s in the theta, beta or gamma frequency band for each electrode and each participant. The data were collapsed over the z-axis and smoothed. The background brain is a slice (z = –16) of the Montreal Neurological Institute standard brain. The pink rectangles outline piriform cortex. The source is available in S5 Data.

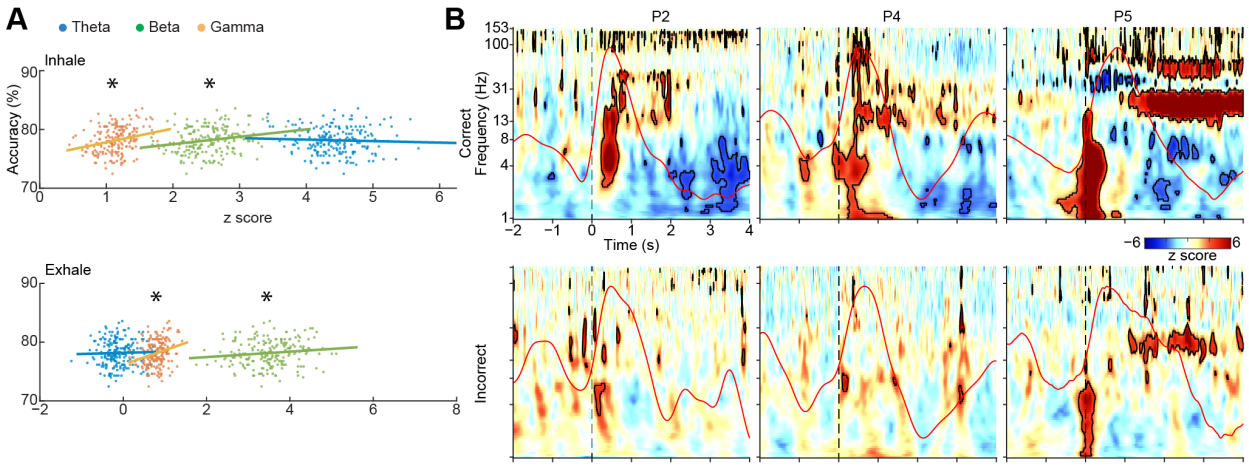

S4 Fig. Related to Fig 4. Odor-induced responses for correct and incorrect trials. (A) Example scatter plots showing the correlations plotted in Fig 4C. The scatter plot corresponding to the correlation value of one dot from each bar in Fig 4C is shown. (B) Representative spectrograms from 3 participants, showing correct (top) and incorrect trials (bottom) separately. The red solid overlay indicates each participant's (P1–P7) respiratory signal. Black outlines indicate statistically significant clusters ($P < 0.05$, false-discovery-rate corrected). The vertical short-dashed line indicates sniff onset. The source is available in S5 Data.

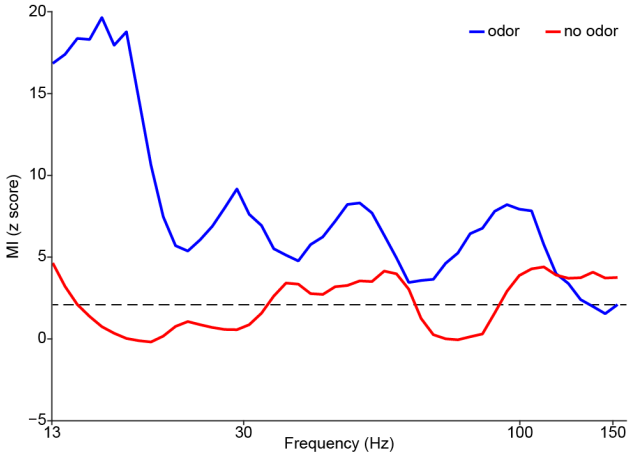

S5 Fig. Related to Fig 6. Results of modulation index computed for odor and no-odor trials, accounting for possible contribution of steep slope of sensory-evoked potentials (see supplementary Methods). The source is available in S5 Data.

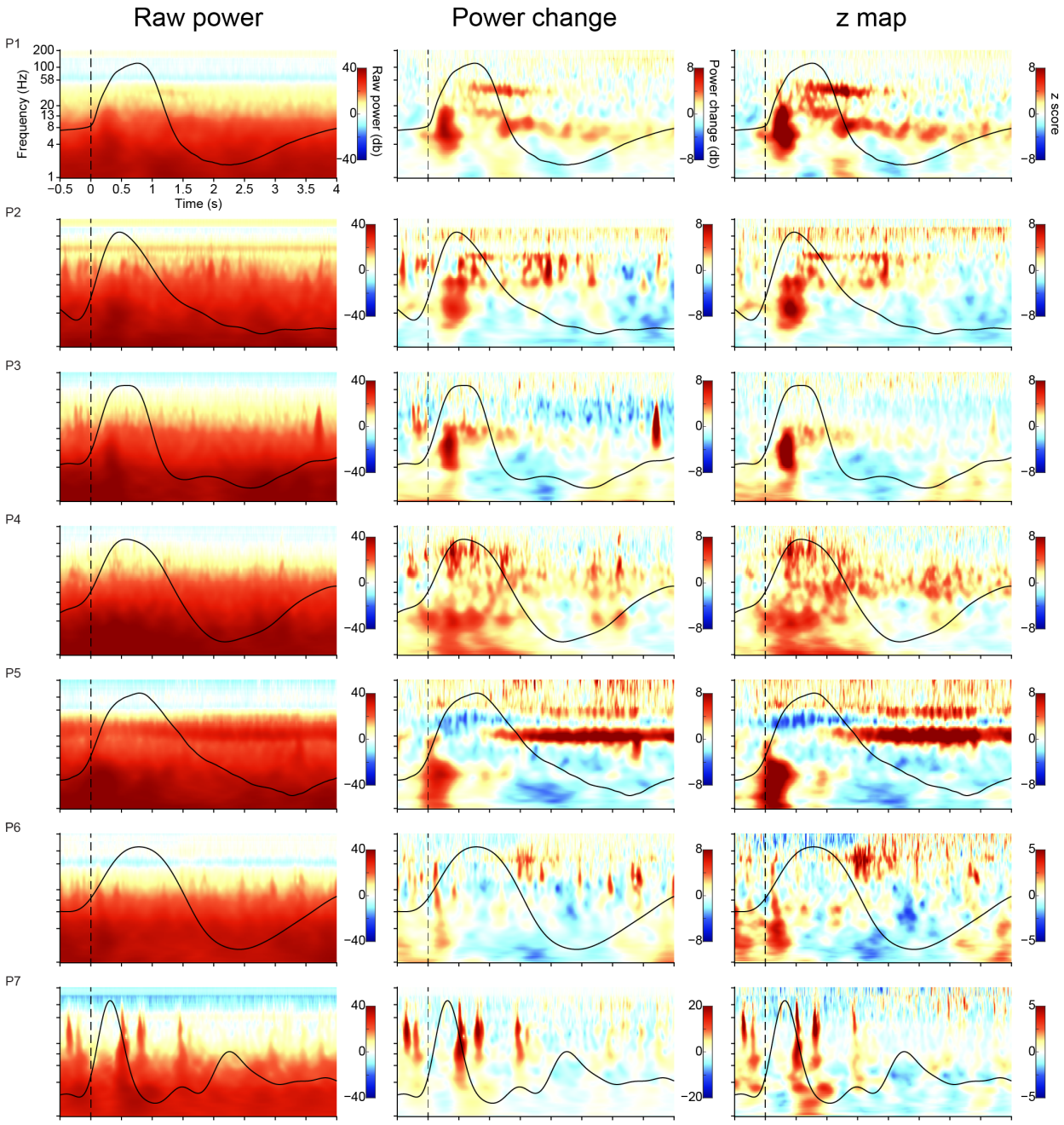

S6 Fig. Related to Fig 2. Sniff-onset aligned raw power (left), power change relative to baseline (middle), and z score map (right, same as Fig 2C) are shown for each participant (P1–P7). The baseline was defined as [–0.55, –0.05] s prior to cue onset.

The black overlaid line indicates the respiratory signal. The vertical short-dashed line indicates sniff onset. The source is available in S5 Data.

S1 Text. Supplementary methods.

S1 Data. Zip file containing datasets underlying Fig 2A, 2B, and 2C.

S2 Data. Zip file containing datasets underlying Fig 3A, 3B, 3C, and 3D.

S3 Data. Zip file containing datasets underlying Fig 4A, 4B, 4C, 4D, and 4E.

S4 Data. Zip file containing datasets underlying Figs 5B, 6A, 6B, and 7.

S5 Data. Zip file containing datasets underlying S1 Fig, S2 Fig, S3 Fig, S4 Fig, S5 Fig and S6 Fig.